Technical Memo

ECMWF
European Centre for Medium-Range Weather Forecasts

923

Indian Ocean teleconnections to the northern extra-tropics: a challenging problem in climate modelling

Franco Molteni and Anca Brookshaw

December 2024

Series: ECMWF Technical Memoranda

A full list of ECMWF Publications can be found on our web site under:

http://www.ecmwf.int/publications/

Contact: library@ecmwf.int

© Copyright 2024

European Centre for Medium Range Weather Forecasts
Shinfield Park, Reading, Berkshire RG2 9AX, England

Literary and scientific copyrights belong to ECMWF and are reserved in all countries. The content of this document is available for use under a Creative Commons Attribution 4.0 International Public License. See the terms at *https://creativecommons.org/licenses/by/4.0/*.

The information within this publication is given in good faith and considered to be true, but ECMWF accepts no liability for error, omission and for loss or damage arising from its use.

Abstract

In the first part of this report, we summarise the state of the art with the regard to the diagnostics and model simulation of teleconnections originated from the Indian Ocean. From a selection of relevant papers in the scientific literature, we point out that similar problems exist when we look at the problem on a range of time scales, from the sub-seasonal to the interdecadal. While the relevance of teleconnections from the Indian Ocean to the northern extra-tropics has become increasingly evident in the last 10-15 years, thanks to both diagnostic studies and specifically planned numerical experimentation, the ability of global numerical models to simulate such teleconnections when they interact with the full range of climate variability has hardly improved in recent years.

In the second part of the paper, we present a range of statistics focussed on the interannual time scale, computed first from observational data (ERA5 and GPCPv3.2 rainfall) and then from the seasonal re-forecasts generated by five European models contributing to the multi-model ensemble of the Copernicus Climate Change Service (C3S). The comparison between observed and simulated teleconnections indicates that current coupled models used for seasonal forecasting can reproduce reasonably well the connections between Indo-Pacific SST and rainfall during the boreal cold season, but (consistently with earlier results) they can only simulate the connections of Indian Ocean SST and rainfall with the North Atlantic/European circulation with about (at best) half the amplitude of the signal from observational data. We also discuss the statistical significance of the differences between observed and model teleconnections, showing that the results are sensitive to the choice of datasets used in the observational diagnostics.

Plain Language Summary

It has been known for decades that variability in the temperature of tropical oceans changes the location and intensity of tropical atmospheric heating (primarily due to changes in rainfall patterns), and in turn these heating anomalies generate Rossby waves which propagate into the extra-tropical regions. While most attention has been devoted to study the impact of the El Niño – Southern Oscillation (ENSO) phenomenon, in the last two decades evidence has been growing on the connections between variability in Indian Ocean temperature and rainfall, and anomalies in the large-scale circulation over the North Atlantic and European region. In this report, we first review the current understanding about these teleconnections and the ability of numerical models to simulate them across a range of time scale. Then, we compare teleconnection patterns derived from observational data with those generated by five state-of-the-art seasonal forecast models. The results show that further progress is needed in the simulation of these phenomena, and that achieving such progress is likely to have a significant positive impact on the skill of seasonal forecasts for Europe.

1. Introduction

When seasonal forecasting with coupled models was started in the 1990s, it was well understood that the main source of seasonal predictability came from anomalies in tropical sea surface temperature (SST), their impact on atmospheric diabatic heating and the consequent changes in the tropical and extratropical circulation (e.g. Palmer and Anderson 1994). With El Niño – Southern Oscillation (ENSO) being the dominant mode of coupled variability, it was natural that early efforts on coupled seasonal forecasting were mainly assessed in terms of their ability to predict ENSO episodes (for the early ECMWF system, see Stockdale et al. 1998). Of course, even today ENSO (and its teleconnections within the tropics and to the extra-tropics) remains the main target of seasonal predictions, in terms of both research work and operational assessment. However, near the turn of the century and the early 2000s, several research groups turned their attention to another source of large-scale teleconnections: the variability of sea-surface temperature (SST) and the tropical circulation over the tropical Indian Ocean.

Although the variability of the circulation over the Indian Ocean had been studied for decades by scientists interested in the dynamics and prediction of the Asian monsoon, the very strong SST anomalies preceding the peak of the 1997-98 El Niño focussed the attention of the scientific community on the coupled phenomenon now known as the Indian Ocean Dipole (IOD; see Saji et al. 1999; Webster et al. 1999). The IOD is, like ENSO, a coupled phenomenon with predominantly interannual variability, although subject to decadal variations in intensity and its relationship to ENSO. After the 1997 episode, much attention was devoted to how the contemporaneous occurrence of ENSO and IOD affected the South Asian monsoon (e.g. Ashok et al. 2001), while the extratropical impacts of the IOD received (at that time) only minor attention.

In the following years, the connection between oceanic and atmospheric anomalies over the Indian Ocean and the variability of the North Atlantic /European was investigated on time scales either shorter or longer than the interannual. On the multi-decadal scale, the companion papers by Hurrell et al. (2004) and Hoerling et al. (2004) suggested that the long-term warming of the Indian Ocean was the main source of the trend towards the positive phase of the North Atlantic Oscillation (NAO) observed in the second half of the 20th century. On the sub-seasonal time scale, observational and modelling studies linked the different phases of the Madden-Julian Oscillation (MJO) to changes in the prevailing anomalies and flow regimes over the North Atlantic (Cassou 2008, Lin et al. 2009), with positive NAO occurrences following the MJO phases with active convection over the Indian Ocean. These studies prompted an extensive assessment of the role of MJO and its teleconnections on the skill of sub-seasonal forecasts (Vitart 2017; Stan et al. 2022), which will be further discussed in the next section.

Interest in the extratropical impacts of Indian Ocean SST and rainfall variability on the interannual scale increased after 2010. Among others, Fletcher and Kushner (2011) and Fletcher and Cassou (2015) investigated the separate impact of Indian and Pacific Ocean SST on the Northern Annular Mode (NAM), pointing out the oppositive effect of teleconnection from the two basins. Molteni et al. (2015) came to similar conclusions when looking at the overall pattern of the North Atlantic teleconnections, noting that teleconnections from the Indian Ocean showed a more significant response when computed using indices of tropical rainfall instead of SST. The interest on this topic surged after (boreal) winter 2019/20, when a very strong IOD episode in the preceding autumn caused significant rainfall anomalies which in turn produced a strong NAO response in the winter (Hardiman et al. 2020).

In view of the mounting observational evidence on the links between Indian Ocean and North Atlantic circulation variability on a range of time scales (all pointing to a shift towards positive NAM / NAO as a result of increased Indian Ocean SST and/or rainfall), it would be desirable to see such teleconnections reproduced in numerical climate models with a high degree of accuracy. As we discuss in the next section, unfortunately this is not the case. Although specific modelling experiments aimed at isolating the impact of Indian Ocean variability have been generally successful in reproducing the observed teleconnection patterns, the Indian Ocean extra-tropical teleconnections appear to be strongly underestimated in their amplitude and significance when predictions and historical simulations including the full range of ocean-atmosphere variability are considered.

Section 2 of this paper gives a brief review of modelling results on this topic, focussed mainly on results from European modelling and prediction groups. Section 3 presents statistics from observational datasets and re-analyses, which summarise the current knowledge on the Indian Ocean teleconnections on interannual time scales and discuss their uncertainty when looking at the interdecadal scale. Section 4 shows results from the re-forecasts of all European seasonal forecast system contributing to the multi-model ensemble (MME) forecasts from the Copernicus Climate Change Service (C3S), discussing how well they reproduce the observational statistics in Sect. 3. Concluding remarks are made in Sect. 5.

2. A summary of modelling and prediction results

2.1. The sub-seasonal scale

Following the paper by Cassou (2008), showing how the frequency of Euro-Atlantic flow regimes is modulated by the occurrence of different MJO phases, a large number of studies have investigated the mechanisms of extra-tropical MJO teleconnections, and in particular their impact on NAO variability. It has been shown that the MJO link to the North Atlantic circulation occurs through both a tropospheric and a stratospheric pathway, with the latter one being more relevant at longer lead times (Garfinkel et al. 2014; Barnes et al. 2019; Domeisen et al. 2020). It was found that MJO teleconnections to the North Atlantic are stronger than average during El Niño events (Lee et al. 2019), and that slow-propagating MJO events lead to stronger teleconnection than fast-propagating events (Yadav and Straus 2017). (The reader is referred to the bibliography included in these papers for a wider review on these topics).

At the same time, many studies investigated how the MJO extra-tropical teleconnections were reproduced in sub-seasonal forecasts. Among many such studies, the works by Vitart (2017) and Stan et al. (2022) offer a multi-model perspective based on forecasts available from the archive of the Subseasonal-to-Seasonal (S2S) project. Although different statistics were used to quantify the agreement between the modelled and observed MJO response, a general conclusion is that (when looking at responses occurred more than two weeks into the forecasts) all models underestimate the amplitude of the extra-tropical teleconnections. Looking in particular at the projection of the forecast composite anomaly onto an EOF-based NAO pattern, three pentads after an MJO phase 3 and 7 (when convection is enhanced over the Indian Ocean and the Western Pacific respectively), Vitart (2017; see figs. 7 and 8) showed that the NAO response in the models where *at best* only about two thirds as strong as the observed one, with the worst results showing an underestimation by a factor or 3 (for MJO phase 3) or no signal at all (for MJO phase 7). Results from Stan et al. (2022), who put more emphasis on the Pacific-North American sector, were partially more optimistic, but overall confirmed the general underestimation of the extratropical teleconnections.

Even though an under-estimation of teleconnection amplitude remains, can we at least detect an improvement in the simulation of MJO teleconnections in more recent versions of global models used for sub-seasonal predictions? Because of the use of different statistics, it is difficult to give a general answer to this question based on existing multi-model comparisons. However, for the ECMWF model we are in a better position, since MJO teleconnections have been investigated in a more consistent way for at least 15 years: therefore, results from Vitart (2017) can be compared with those of an earlier study by Vitart and Molteni (2010) and in two recent and comprehensive studies by Roberts et al. (2023) and Vitart and Balmaseda (2024).

Looking in particular at Figs. 8 and 9 in Roberts et al. (2023) and Fig. 1 in Vitart and Balmaseda (2024), one may conclude that hardly any progress has been made in the simulation of extra-tropical MJO teleconnections. Even though the sign and time lag of the relationship between MJO phases and occurrence of Euro-Atlantic weather regimes is correctly simulated, the amplitude of the signal is still about (or less than) half of the observed one, and there is no sign of the strengthening of teleconnections during El Nino events.

With regard to the processes which may generate the teleconnection errors, Roberts et al. (2023) point to *"(i) insufficient propagation of Rossby wave activity from the Pacific to the Atlantic following MJO phase 3 during El Niño conditions, when the direct tropospheric teleconnection pathway is most active; and (ii) an underestimated response of the stratospheric polar vortex following MJO phase 8 during La Niña conditions, when the indirect stratospheric teleconnection pathway is most active."*. Vitart and Balmaseda (2024) also suggest that multiple processes may be responsible for the teleconnection errors, but show that an important part of the problem is already originated in the tropics: experiments in which wind and temperature values are relaxed towards ERA5 data in the 10N-10S band show a significant improvement in the North Atlantic component of the teleconnection pattern, with a 40% increase in the overall amplitude and nearly a doubling of the NAO projection (see their Fig. 3 and Table 3). They also suggest that biases in the extension of the sub-tropical Pacific jet stream may alter the Pacific Rossby-wave guide in a way that resembles La Niña conditions, when the North Atlantic MJO teleconnections are weaker.

A final remark on the MJO teleconnections: although the impact on the NAO is usually emphasised, the impact on the frequency of the "Atlantic ridge" regime should not be neglected (see again Fig. 8 in Roberts et al. 2023). A reduction of the frequency of this regime following MJO phases 1 to 3 is consistent with the southward shift of the North Atlantic negative height anomaly (with respect to the canonical NAO pattern) in the teleconnections pattern following enhanced convection over the Indian Ocean.

2.2. The seasonal to interannual time scale

Until a few years ago, the impact of Indian Ocean variability on the extratropical circulation on the seasonal to interannual scale had received a relatively modest attention, at least in comparison with the interest on MJO extratropical teleconnections. Since Indian Ocean SST variability is strongly influenced by ENSO, some earlier studies were concerned with the impact of Indian Ocean warming/cooling during warm/cold ENSO events on the total ENSO teleconnections. In one such study, Annamalai et al. (2007) found extratropical responses of opposite sign to prescribed SST anomalies in

the tropical Indian and Pacific Oceans. Fletcher and Kushner (2011) focused on the impact of Indian and Pacific Ocean anomalies on the Northern Annular Mode (NAM), again finding opposite responses to warming in the two basins, with positive/negative NAM phases being induced by warming in the Indian/Pacific Ocean. These findings were confirmed in a later study by Fletcher and Cassou (2015).

Molteni et al. (2015) noted that the extratropical response to tropical Indian Ocean conditions was captured more effectively by looking at covariances with tropical rainfall, rather than SST, since the diabatic heating over the Indian Ocean is not so strongly constrained by SST as in the central tropical Pacific. They showed that the anomalous heating over the western and central Indian Ocean (WCIO) leads to a positive NAO anomaly in seasonal mean for the boreal winter; such a signal is opposite to the canonical extra-tropical ENSO response in late winter, and is found even when the impact of tropical Pacific anomalies is (linearly) removed in the computation of teleconnections. Comparing results from seasonal reforecasts (from the ECMWF System 4 operational at that time) with those from observational data, they noted that the model response was in phase with the observed teleconnection, but its amplitude was about half as large as in the observed pattern. No improvement in the Indian Ocean teleconnection was noted with the introduction of the ECMWF SEAS5 (Johnson et al. 2019), even though the late-winter extratropical teleconnections from ENSO were improved in the updated system.

The interest in seasonal teleconnections from the Indian Ocean (IO) to the North Atlantic/European (NAE) region grew significantly after a strong positive IOD anomaly in the (boreal) autumn of 2019 was followed by a large, positive NAO anomaly in the following winter. Two notable facts about this event were the absence of significant ENSO-like SST anomalies, and the relatively good skill of seasonal forecasts from several models initialized in late autumn (Lee et al. 2020). Using both observational data and experiments with the GloSea5 model of the UK Met Office, Hardiman et al. (2020) concluded that *"the IOD was a key driver of the observed positive NAO*". From their model experiments, they detected *"two teleconnection pathways of the IOD to the north Atlantic: a tropospheric teleconnection pathway via a Rossby wave train travelling from the Indian Ocean over the Pacific and Atlantic, and a stratospheric teleconnection pathway via the Aleutian region and the stratospheric polar vortex."* The existence to both a tropospheric and a stratospheric pathway is indeed in agreement with what found for the MJO teleconnections originated from the Indian and West Pacific Ocean regions. However, even if the extratropical predictions from GloSea5 for that winter were quite successful (in comparison to those of other European forecast models), the amplitude of the predicted NAO signal was only half of the observed msl pressure anomaly in the NAE region.

The impact of significant SST anomalies in the Indian Ocean on the wintertime NAE circulation was recently investigated by Senan et al. (2024) using prescribed-SST experiments with the ECMWF seasonal forecast model, focusing on the three winters 1997/98, 2015/16 and 2019/20 which had different combinations of IOD and ENSO anomalies. A strong NAO response to warm SST anomalies in the WCIO region was found for all three winters in experiments where only the Indian Ocean SST were modified, with a significant stratospheric pathway for the teleconnection. In reality, the total anomaly was determined by a combination of signals from different regions, with (as in previous studies) the tropical Pacific leading to NAO and stratospheric anomalies of opposite signs to the IO signal. Even in winter 2019/20, in the absence of strong ENSO anomalies, the total NAE anomaly reproduced by the model forced with global observed SST was smaller than the response to the IO SST alone.

With regard to the interference between IO and ENSO signals, it should be noted that results for the whole winter season may be misleading, since this phenomenon shows a significant sub-seasonal variability: Abid et al. (2021) showed that the IO contribution is particularly strong in early winter, when it actually *positively correlated* with the NAE response from the tropical Pacific (see also Molteni and Brookshaw 2023); conversely, the late-winter response to ENSO is (statistically) independent from IO anomalies. It is also worth noting that Abid et al. (2021) were able to simulate a realistic response to anomalous IO heating in early winter even with an atmospheric model of intermediate complexity.

As for the MJO teleconnections, the reduced amplitude of the IO interannual teleconnections is a common problem among state-of-the-art coupled models (see Molteni et al. 2020). Hodson et al. (2022) used an optimal detection method to identify predictable signals over the North Atlantic region in seasonal forecasts for the boreal winter run with UK Met Office GloSea5 system. They identified two leading predictable modes; one of them, prevalent during the December-January period, has an NAO-like pattern and *"is driven at least partly by Indian Ocean sea-surface temperatures"*. They found that *"the signal-to-noise problem in GloSea5 is primarily a feature of the December–January NAO-like mode, with the observed mode being three times larger than in the model."*

The mechanisms linking Indian Ocean variability in SST and rainfall, and their connection with North Atlantic circulation anomalies, was further investigated by Raganato et al. (2014). Using re-analysis data, they found a relationship between the IOD SST index in October and WCIO rainfall in December, as well as with the December NAO index and the associated rainfall and temperature anomalies over Europe. The propagation of the extratropical teleconnection pattern appears to be reinforced by transient eddy feedback over the North Pacific and North Atlantic. When looking at ECMWF SEAS5, they found (as in previous studies) that these processes were reproduced in the model with significantly reduced magnitude.

Putting the findings of all these studies together, one gets the following picture. In late autumn and early winter, IOD and ENSO variability generate rainfall anomalies over the Indian Ocean which have usually a dipolar structure, with positive rainfall anomalies in the WCIO region and negative rainfall anomalies over the Maritime Continents. In turn, by interacting with the Asian-Pacific subtropical jet, this anomalous heating pattern generates a Rossby-wave source, from which a Rossby wave propagates into the North Pacific and then in the North Atlantic. In addition to the tropospheric propagation, the North Pacific anomaly modifies the heat fluxes into the lower stratosphere; the consequent change in the strength of the polar vortex acts as an additional forcing for NAO-like anomalies. While all these processes have been reproduced in model simulations, realistic amplitudes for the North Atlantic signals have only been obtained in idealized experiments in which specific anomalous forcing have been applied in the Indian Ocean region. However, when the IO anomalies interact with a variety of other sources of variability in coupled seasonal forecasts or multi-decadal historical simulation, the signal from the Indian Ocean appears to be strongly weakened in comparison with the observed teleconnections. The reasons for such model deficiencies are far from being properly understood.

2.3. Inter-decadal variability and trends

Although the extratropical impacts of IO variability on decadal time scales are reviewed here after those on shorter time scales (which are more relevant to the ECMWF mission), the interdecadal changes occurred in the second half of the 20th century were actually the phenomena that first brought the Indian Ocean – North Atlantic connections to the attention of the scientific community. One of the first influential works on this topic is the paper by Hoerling et al. (2001), in which they compare statistics of SST data and NAO indices for the 1950-1999 period with the results of simulations performed with the NCAR CCM3 model forced by prescribed observed SST. Their results show a remarkable agreement in the phase of the NAO decadal variability between observation and model simulations, as well in the pattern of the North Atlantic trends, with the ensemble-mean response being about half as strong as in the observations. The results of this study were confirmed in two subsequent papers by the same team (Hurrell et al. 2004; Hoerling et al. 2004), supporting the conclusion that extratropical circulation trends in the last decades of the 20th century were mainly driven the warming of tropical oceans, and pointing specifically to the Indian Ocean warming as the main source of the observed NAO trend.

In the following years, these studies were followed by similar ones which analysed the output of AMIP-type multi-decadal simulations driven by observed SST. One such study, by Sanchez-Gomez et al. (2008), looked at simulations from 5 atmospheric GCMs forced by two SST composites representing the opposite phase of the Indo-Pacific SST trend in the last 50 years of the 20th century. They diagnosed the response in terms of both the mean spatial patterns and the frequency of the four North Atlantic regimes identified by Vautard (1990). Although the average, multi-model response showed, as in earlier studies, an amplitude reduced by about a factor of 2, results from some of the models were reasonably close to observations; however, it should be noted that the difference between the SST composites used for the simulations was, by construction, almost twice as large as the average observed SST change between the two periods used to compute the observational statistics.

It should be mentioned that the temporary reversal of the wintertime NAO/NAM trend during the so-called “hiatus” or ”slowdown” in global warming in the first decade of the 21th century (e.g. Trenberth and Fasullo 2013) reduced somehow the interest of the scientific community on this topic, since the continuous Indian Ocean warming was not reflected in the NAO statistics. However, if one looks on a longer time scale, a positive NAO/NAM trend can still be detected over the last 70 years, as argued by Jeong et al. (2002). Also in this paper, results from recent AMIP-type model simulations for the last 6 decades were compared with the observed record, specifically using an Arctic Oscillation (AO) index based on msl pressure; and again, the multi-model mean trend was found to have about half the amplitude of the observed trend, with the North Atlantic signal coming predominantly from Indian Ocean SST.

With results from historical simulation (both coupled and with prescribed SST) from the CMIP6 framework being now available, one may wonder if any progress has been made in recent years in the simulation of trends in the wintertime North Atlantic circulation. Such a study is clearly beyond the scope of this paper; however, a sample of historical simulations following the HighResMIP protocol (Haarsma et al. 2016), run by European institutions under the PRIMAVERA EU-funded project, were diagnosed in the study by Molteni et al. (2020). In addition to confirming the difficulty of current global

models in reproducing the IO teleconnections, the authors looked briefly at the extra-tropical interdecadal changes simulated in the prescribed-SST runs. Results from both a 6-member ensemble with the ECMWF model (see Roberts et al. 2018) and a 6-member multi-model ensemble (shown in their Fig. 15) were not encouraging: the interdecadal change in the NAO index simulated by the MME was only one third of the observed one, while the interdecadal changes in the ECMWF ensemble looked like a late-winter El Niño response, with a small but negative NAO index. Such poor results may be understood by looking at the simulated interdecadal changes of IO rainfall in these runs, which were spatially uncorrelated (even of opposite sign in the WCIO region) with the signal found in calibrated rainfall from the CERA20C re-analysis (Laloyaux et al. 2018). Although results from couple simulations were only slightly better on average, at least one model (HadGEM3) with a more realistic simulation of Indian Ocean rainfall reproduced a significant positive change in the NAO phase.

In summary, in contrast to mounting evidence from observational studies and dedicated numerical experiments, serious common problems are found in the model simulation of teleconnections from the tropical Indian Ocean to the North Atlantic/European region across a range of time scales:

- The average simulated amplitude of the response is at best 50 to 60% of the observed signal;
- There is little (documented) evidence of improvements in the simulation of these teleconnections in the last 10~15 years, at least for the ECMWF model.

The rest of this paper is devoted to documenting how the latest generation of European seasonal forecast model performs in this respect, with a focus on interannual teleconnections.

3. Indian Ocean teleconnections from ERA5 and GPCP data

As a reference to be compared with results from seasonal forecast models, here we show how the phenomena involved in the seasonal to interannual teleconnections can be quantified using observational datasets. Specifically, we investigate first the connections between SST and rainfall variability in the Indo-Pacific Ocean during boreal autumn and winter, and then the connection between WCIO rainfall and the North Atlantic circulation during the central months of winter. In the following analyses, we use SST, msl pressure and 500 hPa height data from the ERA5 re-analysis (Hersbach et al. 2020), while rainfall data are taken from the latest version (v.3.2) of the GPCP monthly-mean dataset (Huffman et al. 2022; retrieved from https://disc.gsfc.nasa.gov/datasets/GPCPMON_3.2/summary). These datasets cover a common 40-year period, from 1983 to 2022; since IO rainfall is diagnosed in the December-January sub-season, when the teleconnections with the NAO are strongest (see Fig. 2 in Molteni et al. 2020), rainfall anomalies from December 1982 have been added from the earlier version 2.3 of GPCP (Adler et al. 2003).

The methodology used to quantify the teleconnections is the same as in Molteni and Brookshaw (2023). We first compute an index $s(t)$ defined as the average SST or rainfall anomaly in a specific area (or the difference between two areas); this is considered to be the source of the teleconnection. On either a tropical or extra-tropical domain, we compute the regression of a spatially-varying anomaly field $\boldsymbol{A}(x,y,t)$ on the source s :

1) $\boldsymbol{R}(x,y) = \sum_t \boldsymbol{A}(x,y,t)\, s(t) / \sum_t s^2(t)$

and then project each anomaly $\boldsymbol{A}(x,y,t)$ onto the regression pattern $\boldsymbol{R}(x,y)$ in a specific 'target' domain D. From the definition of $\boldsymbol{R}$, it follows that the projection coefficient:

2) $b(t) = \langle \boldsymbol{A}(x,y,t), \boldsymbol{R}(x,y) \rangle_D \; / \; \langle \boldsymbol{R}(x,y), \boldsymbol{R}(x,y) \rangle_D$

where $\langle \rangle_D$ is the spatial inner product on the domain D, can be written as:

3) $b(t) = s(t) + \varepsilon(t)$

where $s(t)$ is again the source index and $\varepsilon(t)$ is a term, temporally uncorrelated with $s(t)$, which represents the deviation from an exact linear relationship between the source index and the amplitude of the response (as defined by the projection of $\boldsymbol{A}$ onto $\boldsymbol{R}$). For any region D, we can therefore measure the strength of the teleconnection by two indices:

- the root-mean-square (rms) amplitude of the regression pattern $\boldsymbol{R}(x,y)$ within D;
- a signal-to-noise (S/N) ratio defined as rms$\{s(t)\}$ / rms$\{\varepsilon(t)\}$

We first apply this methodology to look at the (contemporaneous) relationship between ENSO SST variability (quantify by the SST anomaly in the Nino3.4 region, 170W-120W, 5S-5N) and the Indian Ocean rainfall in December-January (DJ) 1982/83 to 2021/22. The left column of Fig. 1 shows the regression patterns of SST and rainfall on the Nino3.4 index (normalised by its standard deviation). These patterns have been shown in many previous studies, and are characterised by the horse-shoe shape of the negative SST and rainfall anomalies extending north-eastward and south-eastward from the Maritime Continents. It is worth noting that while the whole tropical Indian Ocean (between 40E and 120E) is covered by positive SST anomalies, the boundary between positive and negative rainfall anomalies is located around 90E, emphasising the tri-polar structure of the rainfall anomaly across the whole Indo-Pacific.

The strength of the relationship between the Nino3.4 index and the tropical IO rainfall (in the region 40E-120E, 15S-15N, shown as a grey box in Fig.1) can be measured by looking at the scatter diagram on the right-hand side of Fig. 1, where the projection of yearly rainfall anomalies onto their regression pattern are plotted against the Nino3.4 index. The S/N ratio of 1.06 is indicative of a fairly clear relationship, albeit with a strong dispersion for La Niña events.

Fig. 2 is the equivalent of Fig. 1, but measuring the delayed effect of the SST IOD in October-November (ON) on the December-January rainfall (as argued in Raganato et al. 2024). Interestingly, here one finds a closer the correspondence between the sign of SST and rainfall anomalies in the two regression patterns (see the region west of Sumatra); overall, the rainfall regression pattern is very similar to the one for Nino3.4 (apart from the strength of the central Pacific anomaly), mainly a consequence of the frequent co-existence of IOD and ENSO events of the same polarity. However, the large S/N ratio and the absence of 'outliers' for strong IOD events in the scatter plot, together with the better correspondence with the ON SST, suggest that following IOD events the IO rainfall anomaly in DJ is mainly a result of the forcing by SST in the preceding autumn months, generating an anomaly pattern which persists into early winter. (Indeed, the regression pattern of ON rainfall on the IOD, not shown, is almost identical to the pattern for DJ rainfall).

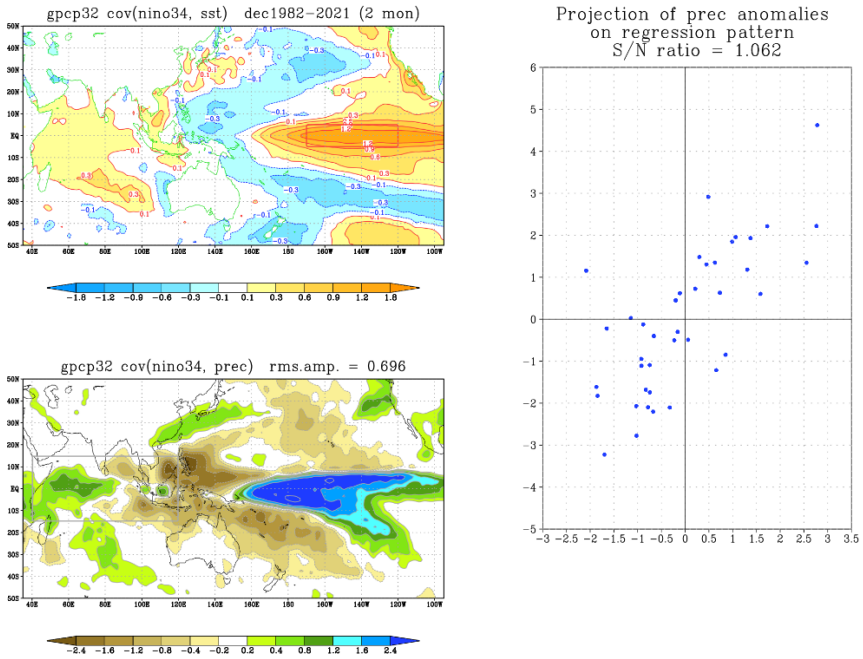

Figure 1: *Left: Regression of Indo-Pacific SST (top) and rainfall (bottom) on the normalised Nino3.4 index in DJ 1982 to 2021. Right: projections of Indian Ocean rainfall anomalies (over the grey box) in individual years onto the rainfall regression pattern, plotted against the normalised Nino3.4 index. SST data from ERA5, rainfall data from GPCPv3.2.*

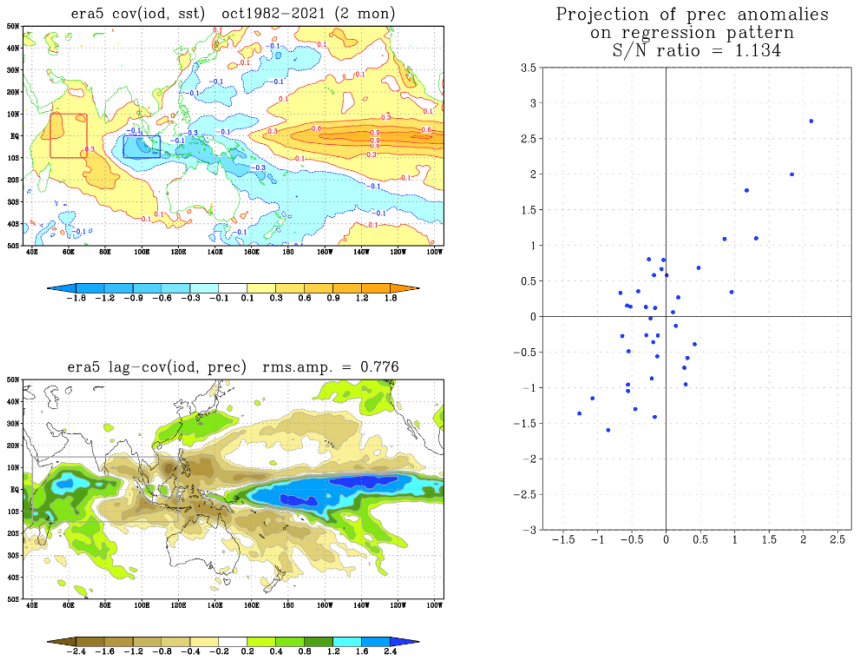

Figure 2: *As in Fig.1, but for the regressions of ON SST (top) and DJ rainfall (bottom) on the normalised IOD index in ON 1982-2021.*

We now look at the extratropical teleconnection originated in the Indian Ocean. Our diagnostics here follow those of Raganato et al. (2024), with the difference of being derived from 2-month means and the additional computation of S/N ratios. Starting from the contemporaneous relationships with WCIO rainfall, Fig. 3 shows the regression pattern of Northern Hemisphere msl pressure and 500-hPa height on the normalised WCIO rainfall index in DJ. Both teleconnection patterns show a clear positive-NAO anomaly, with the negative and positive centres located very close to Iceland and Portugal respectively (as in the traditional NAO definition by Hurrell, 1995). However, while the North Atlantic component dominates the msl pressure patter, in the 500-hPa height teleconnection the NAO signal is embedded in a planetary-scale wavenumber-2 pattern, with a second negative centre near the Bering Strait and positive anomalies covering the sub-tropical west Pacific. The bottom part of the figure shows the scatter diagrams for the projections of the two fields onto their respective regression patterns over the NAE region (70W-30E, 25N-80N), marked in grey in the figure. As expected, the dispersion with respect to a linear relationship with the WCIO index is larger than in the case of the tropical SST vs. rainfall connections discussed above, with the S/N ratio close to 0.68 for both fields.

If WCIO rainfall (and the wider Indo-Pacific rainfall pattern in which it is embedded, shown at the top of Fig. 3) is determined to a significant extent by the IOD anomaly in the preceding autumn, then we should expect the lagged regressions of Northern Hemisphere fields in DJ on the ON IOD to look similar to the WCIO teleconnections. The IOD lagged teleconnection patterns and the associated scatter diagrams for the NAE projections are shown in Fig. 4. The similarity with the WCIO teleconnection is evident, the main difference being the stronger Pacific component in the msl pressure pattern. However, as far as the NAE connections are concerned, the IOD teleconnection show a smaller rms amplitude and S/N ratios than the WCIO teleconnections (with a reduction of about 30% for the amplitude and 25% for the S/N ratio), indicating that they arise as a ‘secondary’ effect of the IOD influence on Indian Ocean rainfall during the winter months.

It is well known that the NAO anomalies have a significant impact on the distribution of European rainfall. The above results suggest that the WCIO and IOD teleconnections should also impact on European rainfall. This is indeed confirmed by the teleconnection patterns and scatter diagrams in Fig. 5, where the scatter diagrams refer to a European-only domain (20W-30E, 30N-80N). It is worth noting that the S/N ratio for both the WCIO and IOD teleconnections with European rainfall are stronger than the corresponding values computed from NAE anomalies of msl pressure and 500-hPa height. In particular, the (positive/negative) WCIO rainfall anomaly appears as a strong “predictor” of wet/dry conditions over northern Europe and dry/wet conditions over the Mediterranean countries, with a S/N ratio of 0.85. This highlights the potential benefit of improving the simulation of the WCIO teleconnections in seasonal forecasts.

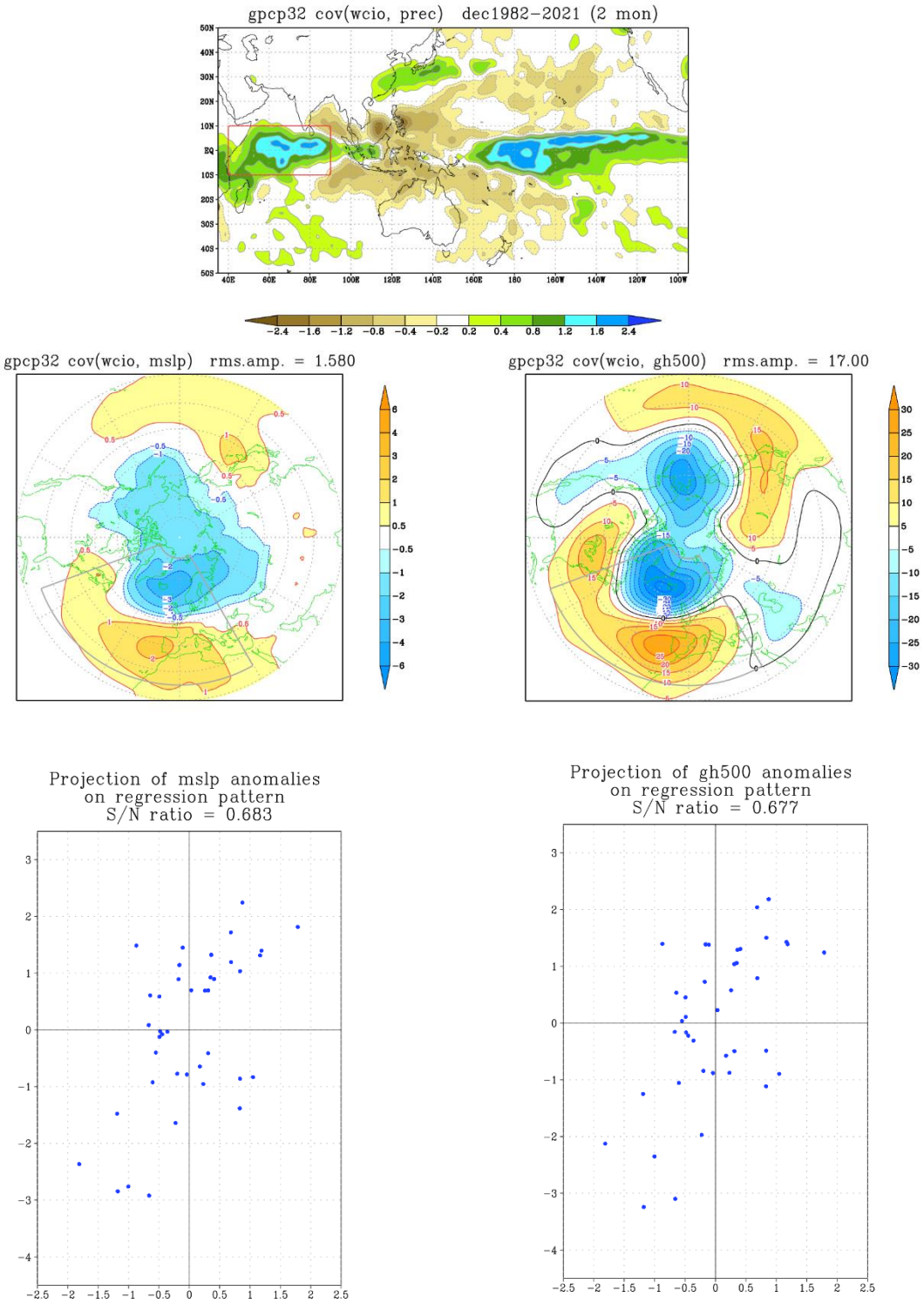

Figure 3: *Regression of Indo-Pacific rainfall (top), N.H. msl pressure (centre left) and N.H. 500-hPa height (centre right) on the normalised WCIO rainfall index (red box) in DJ 1982 to 2021. Bottom row: projections of N. Atlantic/European anomalies (over the grey box) of msl pressure (left) and 500-hPa height (right) in individual years onto the respective regression patterns, plotted against the normalised WCIO index. Msl pressure and 500-hPa height data from ERA5, rainfall data from GPCPv3.2.*

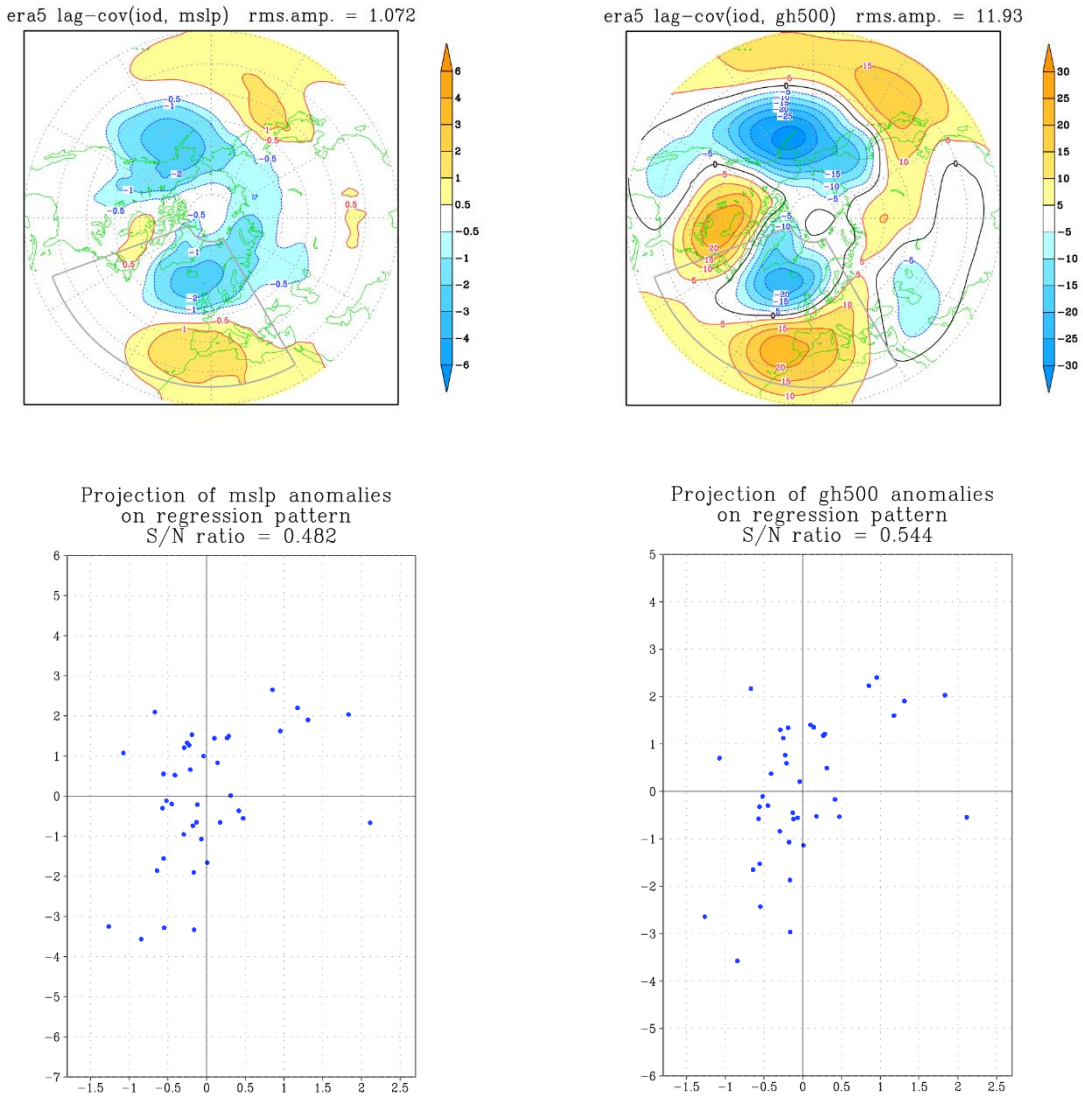

Figure 4: *Top row: Regression of N.H. msl pressure (left) and N.H. 500-hPa height (right) in DJ on the normalised IOD index in ON 1982 to 2021. Bottom row: projections of N. Atlantic/European anomalies (grey box) of msl pressure (left) and 500-hPa height (right) in DJ of individual years onto the respective regression patterns, plotted against the normalised IOD index in ON. Msl pressure and 500-hPa height data from ERA5, rainfall data from GPCPv3.2.*

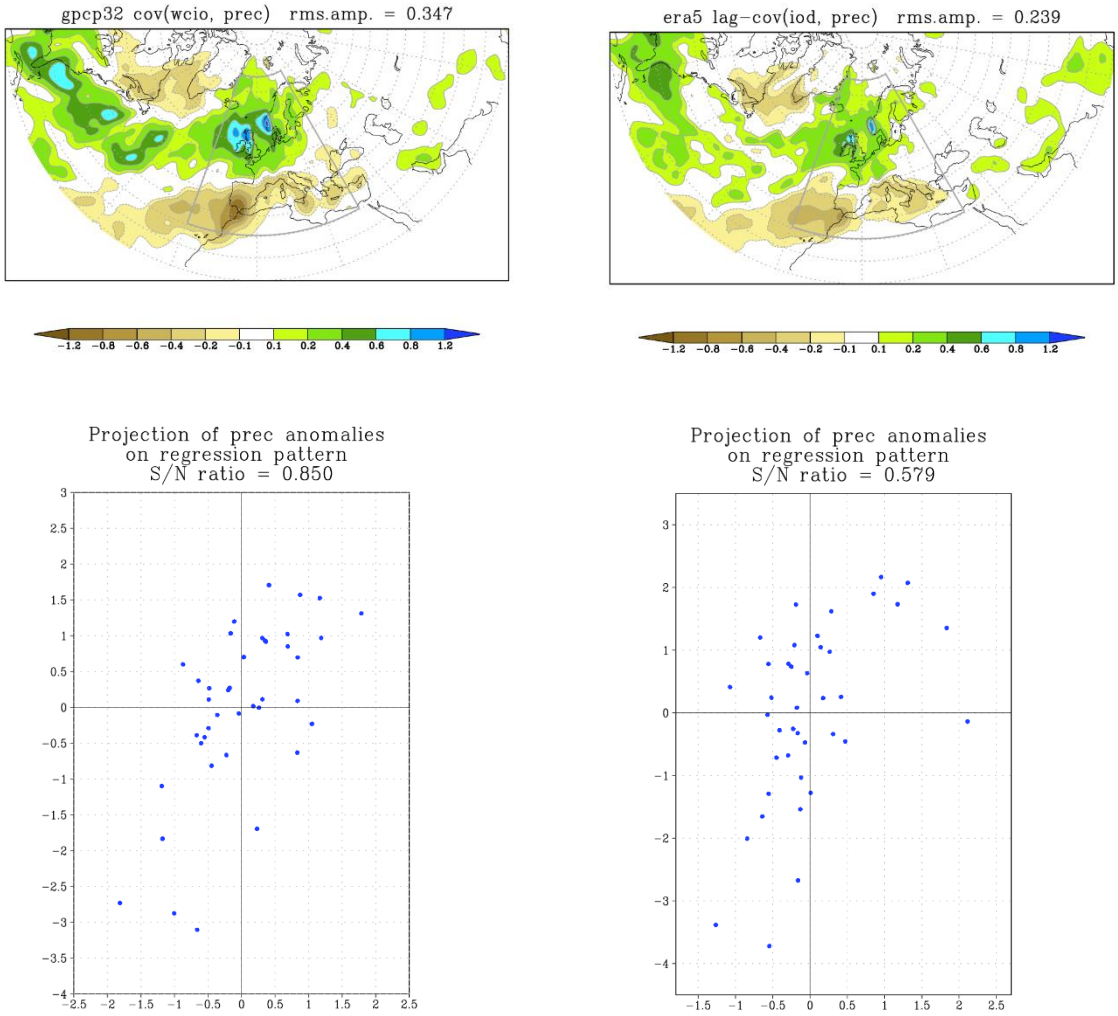

Figure 5: *Top row: Regression of European rainfall in DJ 1982-2021 on WCIO rainfall in DJ (left) and IOD index in ON (right). Bottom left: projections of European rainfall anomalies (over the grey box) in DJ of individual years onto the WCIO regression pattern, plotted against the normalised WCIO rainfall index. Bottom right: as in bottom left, for the projections onto the IOD regression pattern and the IOD index in ON. Rainfall data from GPCPv3.2, SST data from ERA5.*

Before looking at teleconnections in forecast models, it useful to discuss how to assess the statistical significance of the observational results, and their sensitivity to the specific rainfall dataset used in the computation of teleconnections. Given any time series *q(t)* of length comparable to the number of years in the post-1979 satellite era, the regression of atmospheric anomalies on *q* will always show a non-null pattern. And by construction, the projection of individual anomalies onto the regression pattern will be positively correlated with *q*. Therefore, to assess the significance of the relationship between *q* and its apparent 'response', we cannot use tests that assume no correlation as a null hypothesis. We can, however, generate a large number of random time series, and for every such series compute the regression pattern against the *same* atmospheric data used in our teleconnection estimate, its rms amplitude on our domain of interest and the associated S/N ratio. We can then assess what percentage of the random-data statistics exceed the value obtained by regression against the real source index *s(t)*. This is a measure of the significance of the actual teleconnection.

Another source of uncertainty, when we consider multi-decadal rainfall over the tropical ocean, is the reliability of the rainfall data themselves. It is well known that rainfall estimates from reanalyses may show, at least in specific regions, significant differences from product based on raingauge observations or satellite data, which usually get larger going backwards from current times (see e.g. Berntell et al. 2018). Molteni and Brookshaw (2024) have compared rainfall data generated by ERA5 with those obtained from a combination of GPCP data and the data-homogeneous CERA20C analysis over a 72-year period, and have used a combination of principal-component and canonical correlation analyses to filter out signals showing a poor correlation across the two different datasets. To test the sensitivity of our results to the rainfall product used to define the source index, we have re-computed the WCIO teleconnection with 500-hPa height (shown in Fig. 3) using both original and filtered ERA5 data, as well as the filtered GPCP/CERA20C data (ERA5 data of 500-hPa height were used in all cases). Then, we have tested the regression amplitude and S/N ratio over the NAE region against the statistics derived from 1000 random, normally-distributed time series. The results are compared in Table 1 with those of the teleconnection computed from GPCP3.2 data.

	ERA5	ERA5 (filtered)	GPCP3.2	GPCP-CERA20C (filtered)
Rms amplitude	12.8	13.4	17.0	18.5
S/N ratio	0.489	0.534	0.677	0.779
Rms amplitude significance	p = 3.3%	p = 2.4%	p = 0.1%	p < 0.1%
S/N significance	p = 12.3%	p = 6.1%	p = 0.6%	p = 0.1%

Table 1: *Statistics on the regression of N. Atlantic/European 500-hPa height in DJ 1982-2021 on the WCIO rainfall index, using either original or filtered data from ERA5 and GPCP.*

The results show that the WCIO teleconnections computed from ERA5 data (even after filtering) are weaker than the one from GPCP3.2, with a reduction of about 25% in both rms amplitude and S/N ratio when the original ERA5 data are used. This brings a substantial change in the estimate of significance: the probability that the ERA5 results arise from random sampling is more than 20 times larger than the corresponding probabilities for the GPCP3.2 teleconnection. Although the ERA5 teleconnection exceeds the 95% confidence threshold in terms of rms amplitude, it does not exceed 90% confidence when the S/N ratio is considered. While the CCA-filtering improves the ERA5 statistics to a small extent, the filtered GPCP-CERA20C data show an even-stronger relationship with the 500-hPa height anomalies, with S/N ratio increasing from 0.68 to 0.78, and a further increase in the confidence level for the results (only one of the 1000 random time series had a larger S/N ratio, and none had a larger rms amplitude).

To show the impact of the differences discussed above on the actual teleconnection pattern, Fig. 6 shows the WCIO teleconnection computed from the original ERA5 data and the filtered GPCP-CERA20C data, which produce respectively the weakest and the strongest teleconnection. Despite the notable difference in amplitude, the two patterns are remarkably well correlated with each other, as well as with the GPCP3.2 teleconnection in Fig.3; this suggest that the difference between the ERA5 and GPCP rainfall index may be due to a more 'noisy' nature of the re-analysis data.

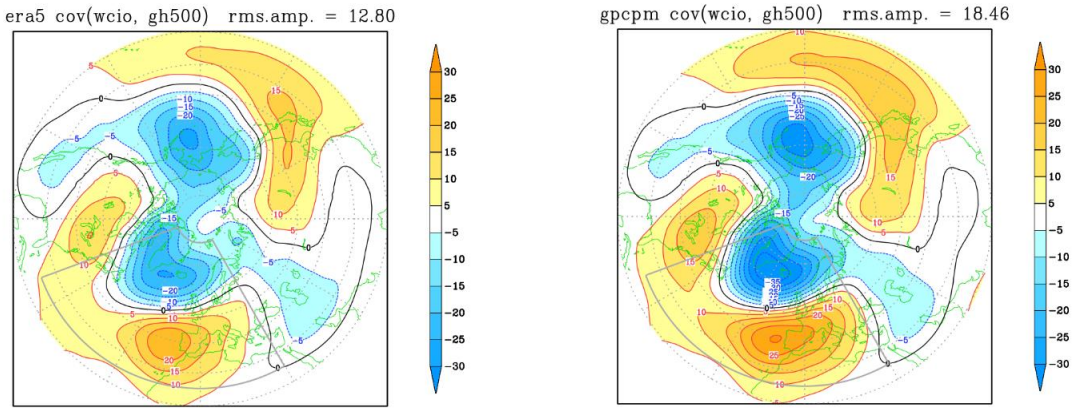

Figure 6: *Regression of DJ 500-hPa height (from ERA5) on the normalised WCIO index in DJ 1982-2021, computed from ERA5 rainfall data (left) or a filtered version of GPCP data (right) where a canonical correlation analysis is used to remove modes of variability uncorrelated with ERA5 data (see Molteni and Brookshaw 2024).*

4. Results from European seasonal forecast models

In this section, we look at how well the European seasonal forecast models contributing to the C3S MME manage to reproduce the teleconnection statistics described in Sect. 3. The seasonal systems considered here are from the following institutes:

- Centro Euro-Mediterraneo sui Cambiamenti Climatici (CMCC)
- Deutscher Wetterdienst (DWD)
- European Centre for Medium-range Weather Forecasts (ECMWF)
- Meteo France
- UK Met Office

For all models, data are derived from re-forecasts started in October 1993-2016, performed with the model version operational in October 2023 (further information on the model versions is found on https://confluence.ecmwf.int/display/CKB/Description+of+the+C3S+seasonal+multi-system). The only exception is made for the UK Met Office model: in the Met Office system, for each nominal initial date the ensemble members are started from 4 different initial days up to 3 weeks apart. Using re-forecasts from the two most recent initial dates (i.e those closer to 1 October) for the three versions of GloSea6 (labelled 600, 601 and 602 in the C3S MME), the lag in initial conditions is closer to that used in other systems, and the teleconnections computed in this way are slightly improved with respect to those derived from the full set of re-forecasts of the 602 version. As discussed by Molteni and Brookshaw (2023), comparing the re-forecast statistics with those from a observational record spanning more years (40 instead of 24) does not affect the validation in a negative way; on the contrary, a longer record allows to reduce the random component in the observed regressions, increasing the consistency with the smoother regressions obtained from the larger samples of ensemble forecasts.

4.1. SST forcing of Indo-Pacific rainfall

We first examine how the seasonal forecast models reproduce the relationship between Indo-Pacific SST and Indian Ocean rainfall. Starting with the results of the ECMWF model, we show in Figs. 7 and 8 the same statistics computed from ERA5 and GPCP data in Figs. 1 and 2 respectively. Looking at the impact of ENSO in DJ (Fig. 7), the similarity between the model and observed regression patterns is excellent for SST; for the rainfall regression, the large-scale east-west gradient is well reproduced, but the model tends to create a meridional asymmetry across the Equator in the rainfall anomalies between 70E and 90E which is not found in the observational data. The regression amplitude and S/N ratio for the tropical IO domain (listed in Table 2) are very close to the ERA5/GPCP results.

Looking at the lagged regression of DJ rainfall on the IOD index in the preceding ON (shown in Fig. 8), the meridional asymmetry already noted in the ENSO regression becomes more evident, with large negative anomalies extending westward from the Maritime Continent into the central Indian Ocean. This feature is likely to be induced by the larger-than-observed SST variability in the eastern Indian Ocean, and particularly in the upwelling region west of Sumatra (the eastern ‘pole’ in the IOD definition), as already documented in Johnson et al. (2019). Overall, the rainfall regression amplitude is about 10% larger than the observed value, and the same is true for the S/N ratio (see again Table 2).

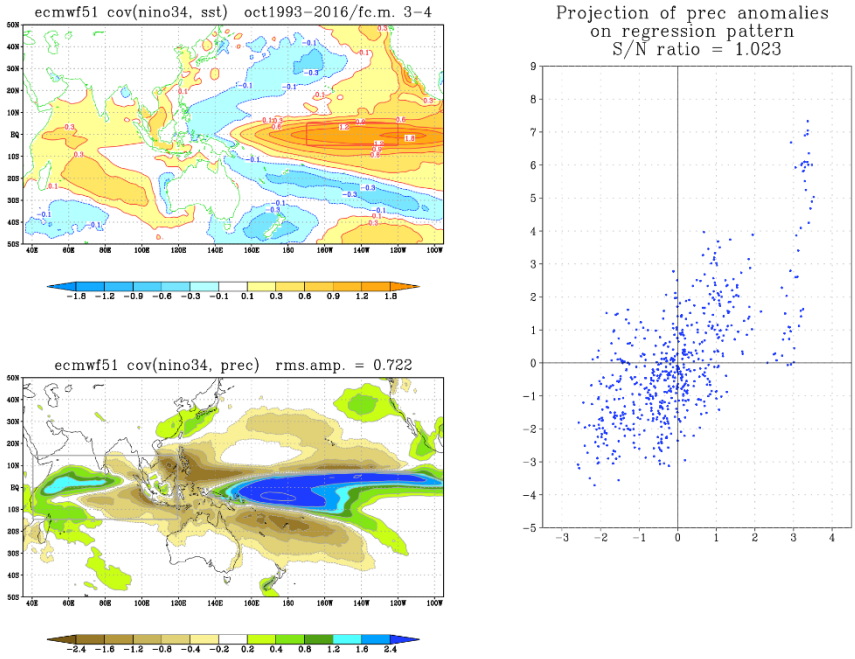

Figure 7: *Left: Regression of Indo-Pacific SST (top) and rainfall (bottom) on the normalised Nino3.4 index in DJ 1993 to 2016, from ECMWF seasonal re-forecasts started on 1 October. Right: projections (over the grey box) of Indian Ocean rainfall anomalies in individual years and ensemble members onto the rainfall regression pattern, plotted against the normalised Nino3.4 index.*

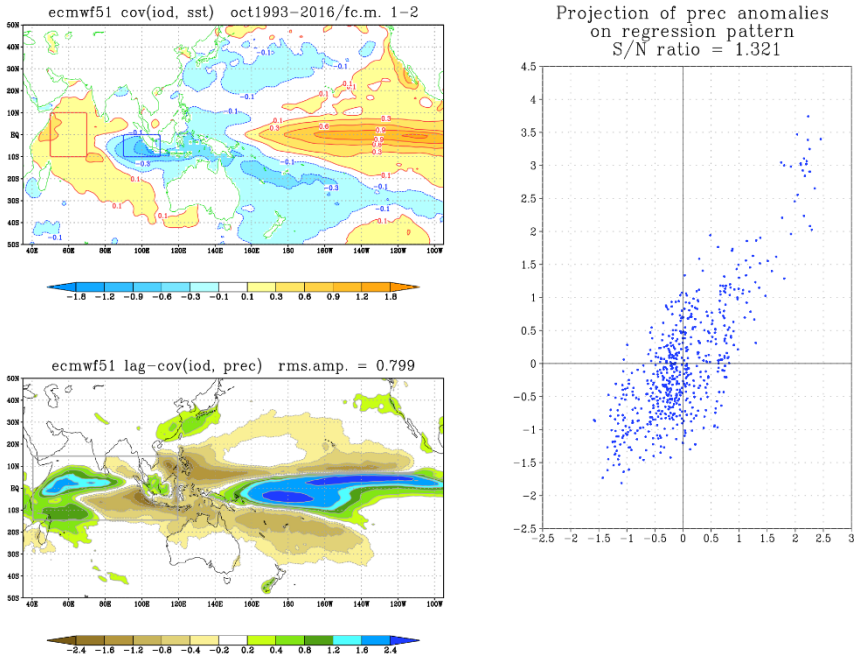

Figure 8: *As in Fig.7, but for the regressions of ON SST (top) and DJ rainfall (bottom) on the normalised IOD index in ON 1993-2016, from ECMWF re-forecasts started on 1 October.*

	ERA5/GPCP	CMCC	DWD	ECMWF	Meteo Fr.	MetOffice
Rms amplitude DJ Nino3.4	**0.70**	0.74	0.44	0.72	0.78	0.89
S/N ratio DJ Nino3.4	**1.060**	1.233	0.924	1.023	1.323	1.229
Rms amplitude ON IOD	**0.72**	0.72	0.50	0.80	0.72	0.90
S/N ratio ON IOD	**1.165**	1.273	1.123	1.321	1.111	1.283

Table 2: *Rms amplitude and S/N ratio for the regression (over the grey box in Fig. 7) of Indo-Pacific rainfall in DJ on the normalised Nino3.4 index in DJ and the IOD index in ON, from ERA5 /GPCPv3.2 and seasonal reforecasts started (nominally) on 1 Oct. 1993-2016.*

The rainfall regressions on the DJ Nino3.4 and ON IOD indices are shown in Fig. 9 for the other models, and the regression amplitudes and S/N ratios are listed in Table 2. All models reproduce a regression amplitude over the Indian Ocean and a S/N ratio similar to the observed values, with the notable exception of the DWD model, which generates significantly weaker IO anomalies associated with both indices. The largest amplitudes are found in the Met Office regressions. While the large-scale east-west differences are simulated by all models (albeit poorly by DWD), the regression patterns differ for the extent of the meridional asymmetry in the central Indian Ocean: this is stronger in the DWD and Meteo France models, much weaker in the CMCC and Met Office simulations. Taking into account the relative strength of positive and negative rainfall anomalies in the WCIO region, all models reproduce a positive average in this region associated with positive ENSO and IOD episodes, with the lagged IOD regression showing (on average) a slightly stronger signal than the Nino3.4 regression.

4.2. Teleconnections to the northern extra-tropics

We now examine the extra-tropical teleconnections simulated by the seasonal forecast models, starting with the Northern Hemisphere circulation anomalies induced by WCIO rainfall. For the ECMWF model, Fig. 10 shows the regression patterns and scatter diagram displayed in Fig. 3 for the re-analysis and GPCP data. While the connection of the WCIO index with rainfall across the Indo-Pacific domain (top panel in Fig. 10) is simulated with realistic amplitude and spatial pattern, the regressions of msl pressure and 500-hPa height have a much weaker amplitude than the observational patterns, even though the positive NAO signal is in phase with the observed one. For both extratropical variables, the statistics listed in Table 3 show that the regression amplitudes over the NAE regions are less than half of the observed values, and the same is true for the S/N ratios.

The regression patterns of msl pressure and 500-hPa height for the other four models are shown in the left and right columns of Fig. 11. The regression amplitudes and S/N ratios over the NAE region are also listed in Table 3. There are large differences among the results of various models. The regressions from the Meteo France model have the largest amplitudes, a clear wavenumber-2 pattern and a realistic NAO component, providing the best simulation among the five models; still, the NAE regression amplitudes from this model only reach 50% of the observed values.

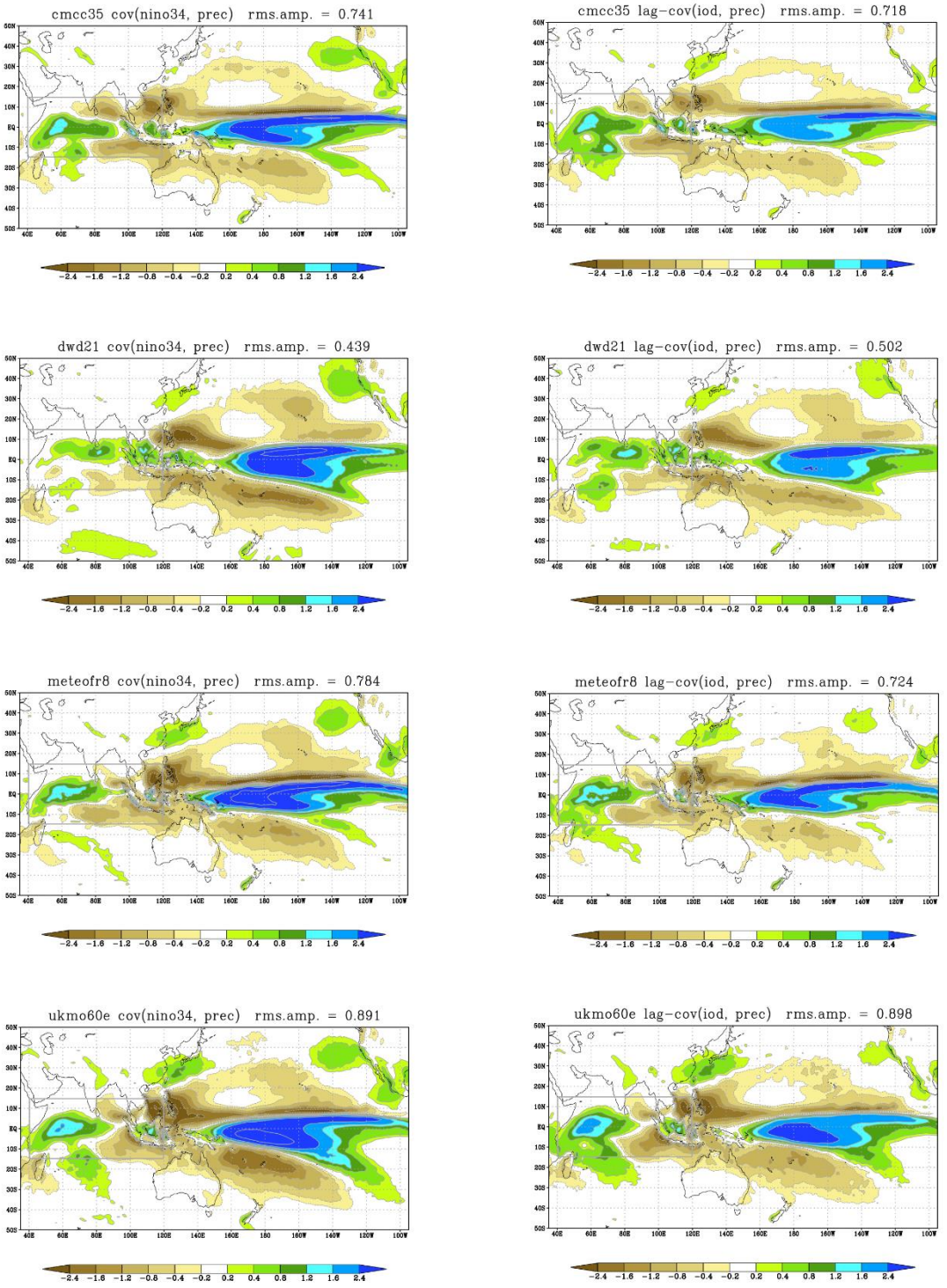

Figure 9: *Regression of Indo-Pacific rainfall in DJ on the normalised Nino3.4 index in DJ (left) and the IOD index in ON (right), from seasonal re-forecasts started (nominally) on 1 Oct. 1993-2016. Top to bottom: from CMCC, DWD, MeteoFrance and UK MetOffice re-forecasts.*

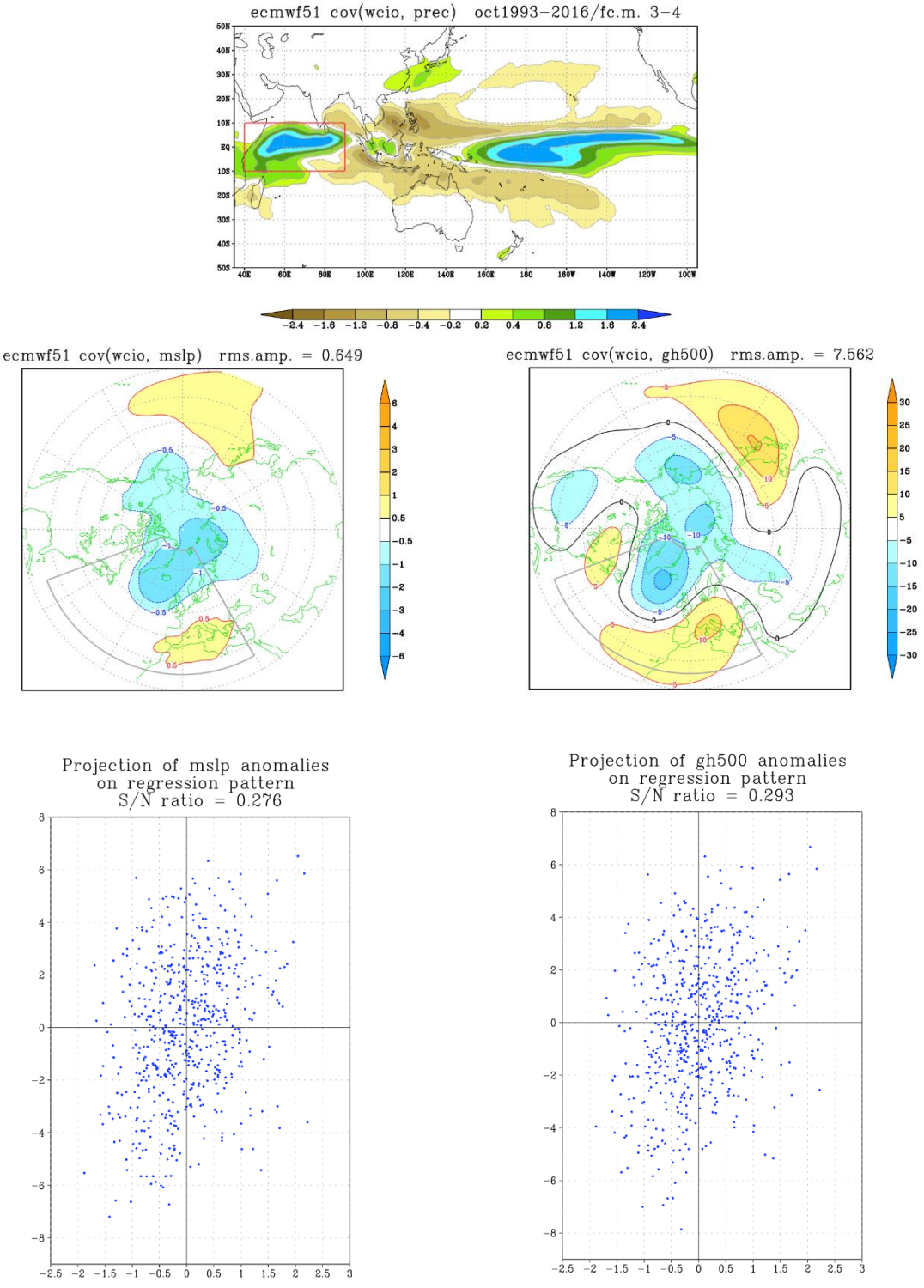

Figure 10: *Regression of Indo-Pacific rainfall (top), N.H. msl pressure (centre left) and N.H. 500-hPa height (centre right) on the normalised WCIO rainfall index (red box) in DJ, from ECMWF seasonal reforecasts started on 1 Oct. 1993-2016. Bottom row: projections of N. Atlantic/European anomalies (over the grey box) of msl pressure (left) and 500-hPa height (right) in individual years and ensemble members onto the respective regression patterns, plotted against the normalised WCIO index.*

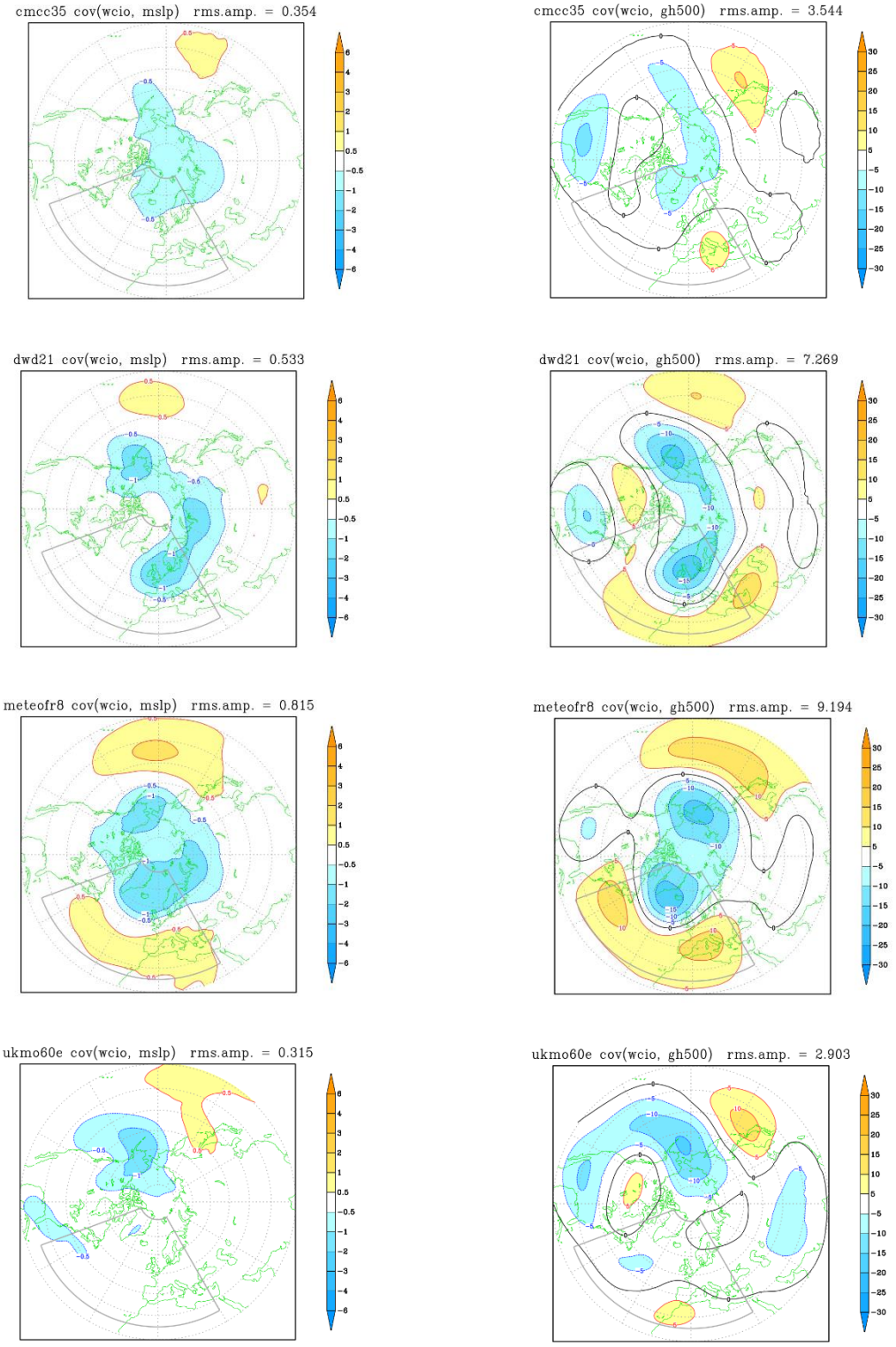

Figure 11: *Regressions of N.H. msl pressure (left) 500 hPa height (right) on the normalised WCIO rainfall index in DJ, from seasonal reforecasts started (nominally) on 1 Oct. 1993-2016. Top to bottom: from CMCC, DWD, MeteoFrance and UK MetOffice re-forecasts.*

The DWD model also produces a wavenumber-2 response, but the negative anomalies on the northern oceans are shifted eastwards in comparison with the observed pattern in Fig. 3. Re-forecasts from the CMCC and Met Office models show a very weak response over the North Atlantic; the results for the GloSea6 system are disappointing when compared to those documented in the literature for earlier versions of the Met Office system.

Looking at the modelled response of Northern Hemisphere fields to IOD variability, we should expect (as in the observations) a rather similar pattern to the WCIO teleconnections, but with reduced amplitude, reflecting the decrease in correlation due to the 2-month lag. For the ECMWF model, the IOD regressions and the projection scatter diagrams are shown in Fig. 12, while for the other models the regression patterns are shown in Fig. 13. The rms amplitudes of the regression patterns and the associated S/N ratios are listed in Table 4.

	ERA5/GPCP	CMCC	DWD	ECMWF	Meteo Fr.	MetOffice
Rms amplitude Msl pressure	**1.67**	0.35	0.53	0.65	0.82	0.32
S/N ratio Msl pressure	**0.712**	0.200	0.324	0.276	0.340	0.256
Rms amplitude 500 hPa height	**17.42**	3.54	7.27	7.56	9.19	2.90
S/N ratio 500 hPa height	**0.689**	0.171	0.388	0.293	0.385	0.216

Table 3. *Rms amplitude and S/N ratio for the regression of N.H. msl pressure and 500-hPa height on the normalised WCIO rainfall index in DJ, from ERA5/GPCPv3.2 and seasonal reforecasts started (nominally) on 1 Oct. 1993-2016.*

	ERA5/GPCP	CMCC	DWD	ECMWF	Meteo Fr.	MetOffice
Rms amplitude Msl pressure	**1.08**	0.19	0.47	0.40	0.34	0.26
S/N ratio Msl pressure	**0.490**	0.208	0.246	0.197	0.178	0.223
Rms amplitude 500 hPa height	**12.13**	2.65	6.64	5.13	4.89	3.08
S/N ratio 500 hPa height	**0.568**	0.222	0.321	0.251	0.267	0.242

Table 4. *Rms amplitude and S/N ratio for the regression of N.H. msl pressure and 500-hPa height in DJ on the normalised IOD index in ON, from ERA5/GPCPv3.2 and seasonal reforecasts started (nominally) on 1 Oct. 1993-2016.*

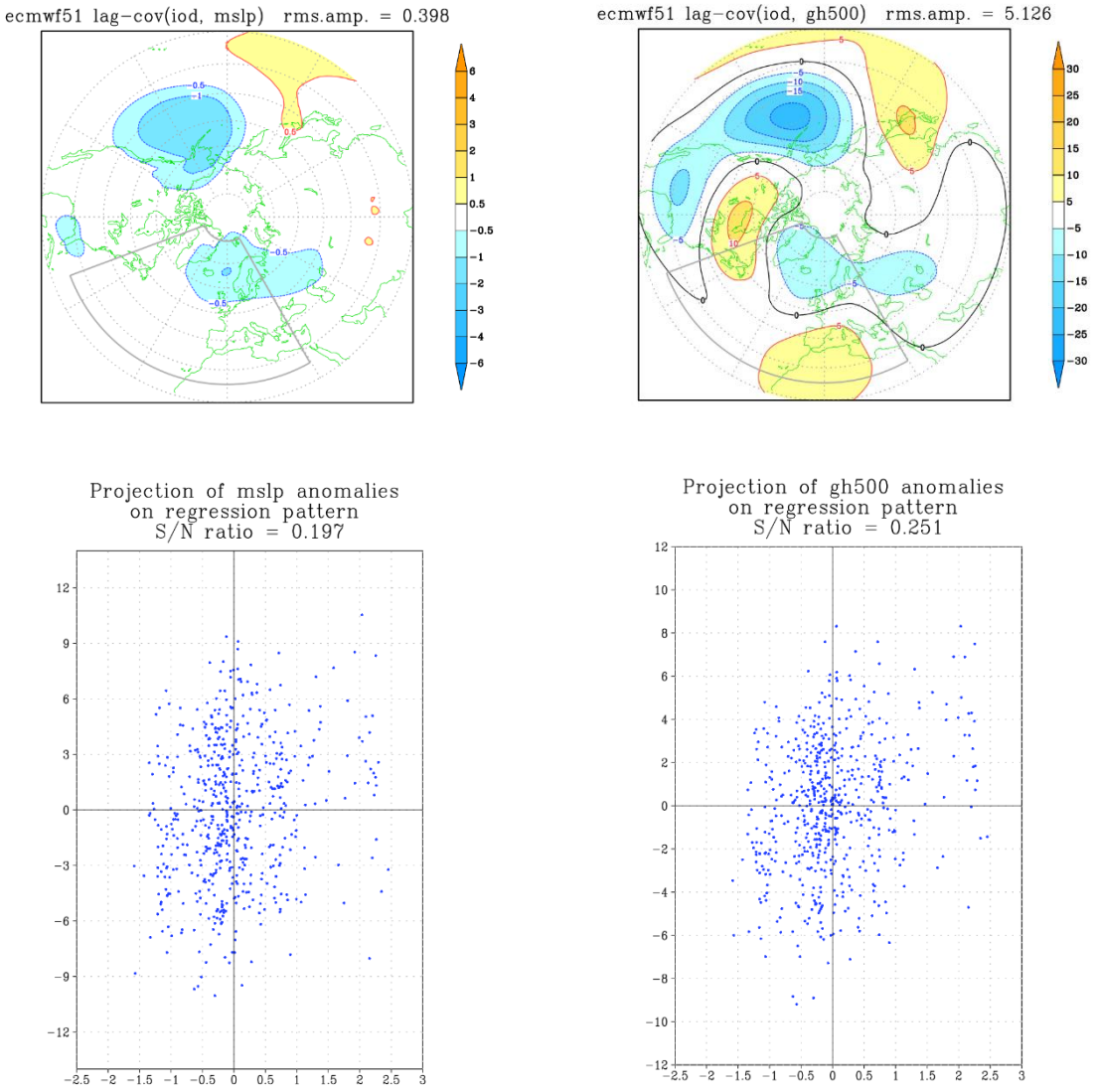

Figure 12: *Top: Regressions of of N.H. msl pressure (left) 500 hPa height (right) in DJ on the normalised IOD index in ON, from ECMWF seasonal reforecasts started on 1 Oct. 1993-2016. Bottom: projections (over the grey box) of msl pressure (left) and 500 hPa height (right) in DJ of individual years and ensemble members onto the respective regression pattern, plotted against the normalised IOD index in ON.*

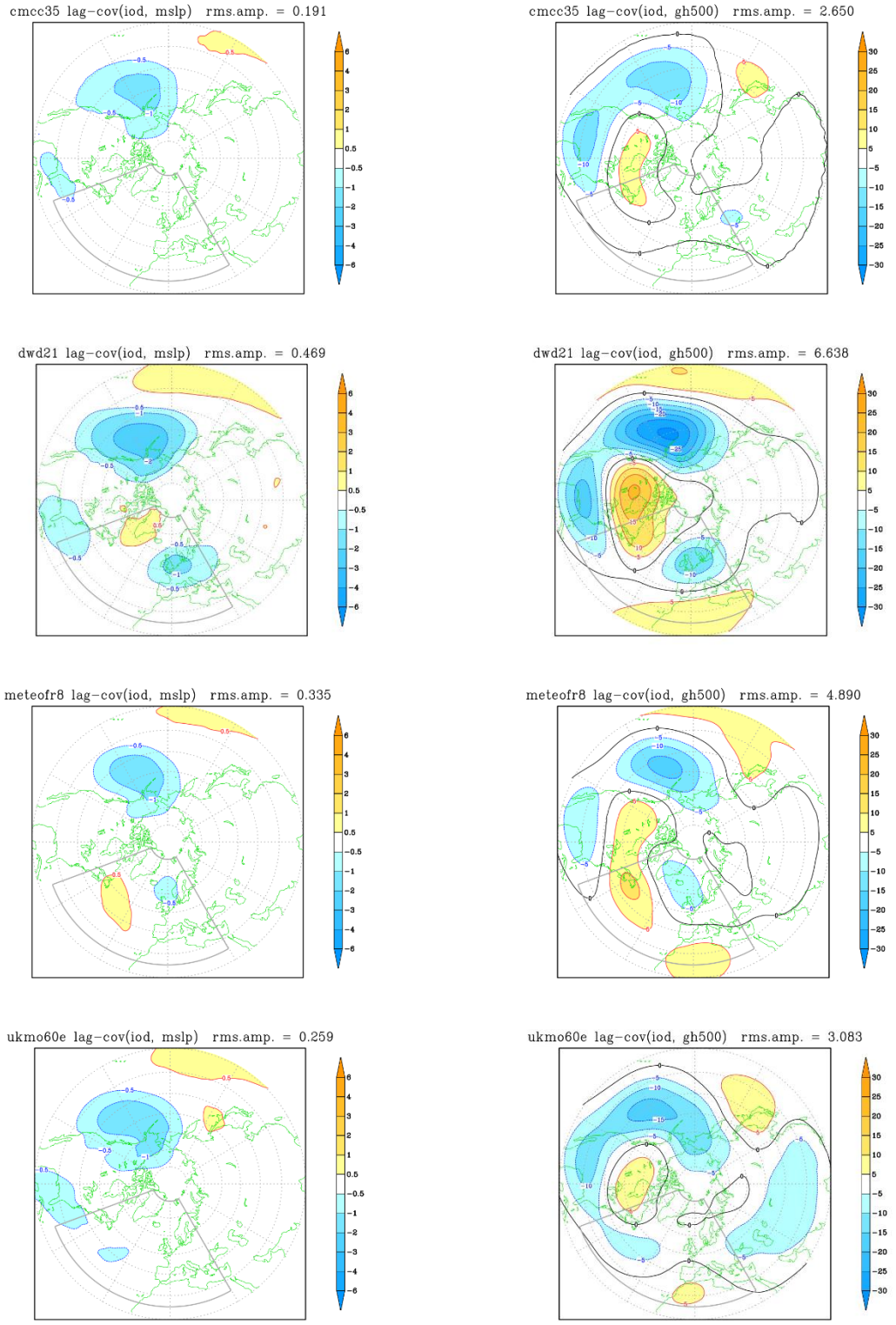

Figure 13: *Regression of N.H. msl pressure (left) 500 hPa height (right) in DJ on the normalised IOD index in ON, from seasonal reforecasts started (nominally) on 1 Oct. 1993-2016. Top to bottom: from CMCC, DWD, MeteoFrance and UK MetOffice re-forecasts.*

Comparing the statistics in Table 3 and 4, we note that in observations the rms amplitudes in the IOD regressions are about 2/3 of those in the WCIO regressions. In the models, this ratio varies between about 0.9 for the DWD to less than 0.5 for the msl pressure response in the CMCC and Meteo France models, although for these models the ratio of the 500-hPa response is closer to the observed ratio.

Overall, one can conclude that the relatively good performance of most models in the simulation of intra-tropical teleconnections is significantly degraded when the extra-tropical teleconnections of Indian Ocean anomalies are considered. In addition, there seems to be little relationship between the performance of individual models over the two domains. For example, the DWD model had clearly the weakest connection between SST anomalies and WCIO rainfall, but its extra-tropical response to the WCIO anomalies is comparable to those of other models. Also, the meridional asymmetry in the central Indian Ocean rainfall discussed in the previous section was hardly visible in the Met Office results, and clearly less pronounced than in the ECMWF tropical regression; still, the ECMWF model performed better in reproducing the WCIO and IOD extra-tropical response.

4.3. Assessing the significance of teleconnection differences

In view of the fact that all models reproduce weaker WCIO and IOD teleconnections than those found in observational datasets, the question arises of whether such differences may be due to observational sampling. In other words, even if we assume that the observed connections are statistically significant (see Table 1), we may hypothesize that random sampling has amplified their strength beyond what is simulated by (at least the most successful) models.

An answer to this question can be found by looking at the distribution of regression amplitudes and S/N ratios obtained by sub-samples of model data of comparable size to the observed record. As an example, we examine the case of the WCIO teleconnection with extra-tropical 500-hPa height in the ECMWF model; since the ERA5 and GPCP record includes 40 winters, we have computed 1000 sub-sampled regressions taking two random ensemble members in each of the 24 re-forecast years, obtaining a slightly larger sample of 48 anomalies. Table 5 shows the median and the 95th percentile of the amplitude and S/N ratio distributions, and the probability that values larger than the observed statistics are obtained from the sub-samples; the latter results are shown comparing model values with those obtained using either ERA5 or GPCPv3.2 data to compute the rainfall anomaly.

As for the overall significance of the “observed” teleconnections shown in Table 1, quite different conclusions can be drawn according to the rainfall dataset used for the comparison. While we cannot rule out with 95% or even 90% confidence that the larger observed signal is simply due to the smaller size of the observed data sample if ERA5 rainfall data are used, there is less than 5% probability that the observed results are compatible with model results from a similar sample size when GPCP data are used to estimate the teleconnections: indeed, such probability is 10 times lower than for ERA5 data, both for the rms amplitude and the S/N ratio.

It is worth noting that the median amplitude and S/N ratio from the 2-member sub-samples are both larger than the values obtained from the full ECMWF sample. This occurs because we are not measuring the projection on a pre-defined pattern for each sub-sample, but we are allowing each sub-sample to generate its own regression pattern.

	median	95th percentile	prob > reg(ERA5)	prob > reg(GPCP)
Rms amplitude	9.6	15.2	16.2 %	1.5 %
S/N ratio	0.435	0.648	31.3 %	3.1 %

Table 5. *Statistics derived from regressions of 500-Pa height in the Euro-Atlantic domain on the WCIO index in DJ, derived of 1000 sub-samples of 48 DJ means obtained from randomly selecting two ensemble members on each year. Data from ECMWF reforecasts started on 1 Oct.*

5. Discussion and conclusions

In this paper, we aimed at summarising the state of the art with the regard to the diagnostics and model simulation of teleconnections originated from the Indian Ocean. From a selection of relevant papers in the scientific literature, we have first pointed out that similar issues are found when we look at the problem on a range of time scales, from the sub-seasonal to the interdecadal. While the relevance of teleconnections from the Indian Ocean to the northern extra-tropics has become increasingly evident in the last 10-15 years, thanks to both diagnostic studies and specifically planned numerical experimentation, the ability of global numerical models to simulate such teleconnections when they interact with the full range of climate variability has hardly improved in recent years.

In the second part of the paper, we have presented a range of statistics focussed on the interannual time scale, computed first from observational data (ERA5 and GPCPv3.2 rainfall) and then from the seasonal re-forecasts generated by the European models contributing to the C3S seasonal MME. The comparison between "observed" and simulated teleconnections has confirmed that current coupled models used for seasonal forecasting can reproduce reasonably well the connections between Indo-Pacific SST and rainfall during the boreal cold season, but they can only simulate the connections of IO SST and rainfall with the North Atlantic/European circulation with about (at best) half the amplitude of the signal from observational data.

We realize that the paper has raised more questions than it has answered, but this was indeed part of our goals. Some of the outstanding issues include:

- What are the causes of the reduced teleconnection amplitudes when ERA5 rainfall are used in the calculations instead of GPCP data? Since the choice of the rainfall dataset affects strongly the estimates of significance, do we have reasons to put more trust in one or another?

- What part do errors in the simulation of Indo-Pacific rainfall play in the under-estimation of the extra-tropical IO teleconnections? Form the statistics presented here, it was hard to relate the model performance in simulating the latter with errors in the intra-tropical teleconnections.

- What is the impact of the deficiencies in IO teleconnection on seasonal predictability for the North Atlantic/European region? How much would we improve our forecasts if such teleconnections were stronger in our model simulations? Or does the unforced variability of Indian Ocean rainfall already represent a barrier for seasonal predictability?

With regard to the last question, a simple argument can be taken as starting point. Since we have shown that the WCIO teleconnection project strongly on the NAO pattern, we can ask ourselves if WCIO rainfall *from the ensemble-mean of seasonal forecasts* is a good predictor of the observed NAO index, and whether we can improve our NAO forecasts by artificially strengthening the WCIO-NAO link in our model. Although any sophisticated statistical scheme would require a careful cross-validation, we can easily build a zero-order model (i.e. with no statistical parameter) by assuming that the linear WCIO teleconnection is the *only predictor* of the NAO in DJ. In this case, our ensemble-mean prediction of the NAO index would be proportional the ensemble-mean WCIO index.

Since the ECMWF SEAS5 system has produced re-forecasts since 1981, and has remained unchanged in the last 7 years, we can look at ensemble-mean predictions of the DJ WCIO and NAO index (the latter is defined here as the difference of msl pressure anomalies in two boxes centred over Iceland and Portugal) for all the 40 winters spanning the 1982/83 to 2021/22 period. Since we are only using DJ data, we can look at seasonal forecasts started on 1 November. Fig. 14 shows the normalised time series of ensemble-mean WCIO, ensemble-mean NAO and observed NAO index from ERA5; the correlations between the three time series (which are not affected by any linear rescaling) are listed on top. While the correlation of the ensemble-mean WCIO index with either the ensemble-mean or the observed NAO index is practically the same (and lower than the correlation of observed WCIO and NAO indices), such a value is actually larger than the correlation between the ensemble-mean and the observed NAO indices. In other words, by assuming the forecast WCIO index as the only NAO predictor we make a better prediction of the observed NAO index than the one made from the msl pressure field in SEAS5 (as far as the ensemble-mean correlation is concerned). This result suggests that the SEAS5 NAO forecasts would be improved if the WCIO impact on the North Atlantic region were stronger, but also that there are further potential gains from improving the prediction of the tropical IO rainfall.

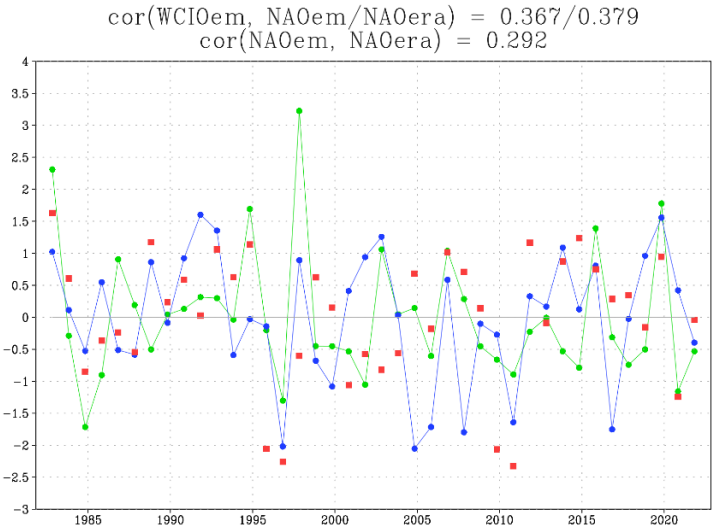

***Fig. 14**: Time series of ensemble-mean WCIO (green line) and NAO (blue line) indices in December-January, from SEAS5 re-forecasts started on 1 November 1982 to 2021, and observed NAO index from ERA5 (red squares). Correlations between the time series are listed above.*

In terms of societal impact, predicting the Indian Ocean teleconnections is not only about getting the NAO index right. As shown in Fig. 5, IO teleconnections are an important factor in shaping the wintertime rainfall anomalies over Europe. This is particularly important for the Mediterranean countries, where available water resources depend largely on the replenishment produced by cold-season rainfall and snowfall. In recent years, winters with prolonged periods of positive NAO anomalies have been followed by severe drought in south-western Europe, with massive impacts on the agricultural production.

In the end, we come back to asking why there has been little progress in the simulation of these teleconnections in long-range forecasts. As suggested by Vitart and Balmaseda (2024), there is a multiplicity of factors affecting the IO teleconnections, and it is difficult to improve them all at the same time. Among the factors already considered in the literature, the current biases in the simulation of eastern Indian Ocean SST, and the difficulty in reproducing the sub-seasonal evolution of the interference between Indian Ocean and central Pacific teleconnections, are some of the most likely sources of error. In addition, we note that the outflow from Indian Ocean convective activity interacts with the South Asian jet across a region of very high and complex topography. Are the topography resolution and the representation of orographic drag affecting the Rossby wave source produced by Indian Ocean rainfall? Can we design specific numerical experiments to address this issue?

Improving the Indian Ocean teleconnections in climate models is not going to be easy; however, for both sub-seasonal to seasonal predictions and climate simulations, we hope to have argued convincingly that it is worth the effort.

Acknowledgements

The contents of this paper arise from discussions and collaborations with many fellow scientists. At ECMWF, we are grateful to all members of the Earth System Predictability Section in the Research Department (the feedback from Chris Roberts and Tim Stockdale was particularly appreciated) and to Laura Ferranti, Chris Goddard, Linus Magnusson and Eduardo Penabad in the Forecasts and Services Department. Long-standing collaborations with Fred Kucharski and Adnan Abid at the International Centre for Theoretical Physics in Trieste, David Straus at COLA/George Mason University in Fairfax (Virginia) and Susanna Corti at the CNR Institute of Atmospheric Sciences and Climate in Bologna have been invaluable. Discussions with Tim Palmer, Antje Weisheimer and other members of the Predictability of Weather and Climate Group in the Atmospheric, Oceanic and Planetary Physics sub-department of the University of Oxford have been a further source of critical thinking and inspiration.

References

- Adler, R.F., and Coauthors (2003) The Version 2 Global Precipitation Climatology Project (GPCP) Monthly Precipitation Analysis (1979-Present). J. Hydrometeor., 4, 1147-1167.
- Ashok K. , Guan Z., Yamagata T. (2001) Impact of the Indian Ocean dipole on the relationship between the Indian monsoon rainfall and ENSO. Geophys. Res. Lett. 28, 4499-4502. https://doi.org/10.1029/2001GL013294
- Barnes, E. A., Samarasinghe S. M., Ebert-Uphoff I., and Furtado J. C. (2019). Tropospheric and stratospheric causal pathways between the MJO and NAO. J. Geophys. Res.: Atmospheres, 124, 9356–9371. https://doi.org/10.1029/2019JD031024
- Berntell, E., Zhang Q., Chafik L., and Körnich H. (2018): Representation of Multidecadal Sahel Rainfall Variability in 20th Century Reanalyses. Sci Rep 8, 10937 (2018). https://doi.org/10.1038/s41598-018-29217-9
- Cassou, C. (2008): Intraseasonal interaction between the Madden Julian Oscillation and the North Atlantic Oscillation, Nature, 455, 523–527.
- Deser, C., and A. S. Phillips, 2006: Simulation of the 1976/77 Climate Transition over the North Pacific: Sensitivity to Tropical Forcing. J. Clim., 19, 6170–6180.
- Domeisen, D. I., Butler A.H., Charlton-Perez A. J., Ayarzagüena B., Baldwin M.P., Dunn-Sigouin E. et al. (2020). The role of the stratosphere in subseasonal to seasonal prediction: 2. Predictability arising from stratosphere-troposphere coupling. J. Geophys. Res.: Atmospheres, 125, e2019JD030923. https://doi.org/10.1029/2019JD030923
- Fletcher, C. G. and Cassou C. (2015) The Dynamical Influence of Separate Teleconnections from the Pacific and Indian Oceans on the Northern Annular Mode. J. Clim. 28, 7985–8002.
- Fletcher, C. G. and Kushner P. J. (2011) The Role of Linear Interference in the Annular Mode Response to Tropical SST Forcing. J. Clim. 24, 778–794
- Garfinkel, C. I., Benedict J. J., and Maloney E. D. (2014). Impact of the MJO on the boreal winter extratropical circulation. Geophysical Research Letters, 41(16), 6055–6062. https://doi.org/10.1002/2014GL061094
- Haarsma R.J., and Co-Authors (2016): High resolution model intercomparison project (HighResMIP v1.0) for CMIP6. Geosci Model Dev, 9, 4185–4208. https://doi.org/10.5194/gmd-9-4185-2016
- Hardiman, S. C., Dunstone N. J., Scaife A. A., Smith D. M., Knight J. R., Davies P., et al. (2020). Predictability of European winter 2019/20: Indian Ocean Dipole impacts on the NAO. Atmospheric Science Letters, 21(12). https://doi.org/10.1002/asl.1005
- Hersbach H. and Coauthors (2020) The ERA5 global reanalysis. Q J R Meteorol Soc. 146, 1999–2049. https://doi.org/10.1002/qj.3803
- Hoerling M.P., Hurrell J.W., and Xu T. (2001) Tropical origins for recent North Atlantic climate change. Science, 292, 90-92. https://doi.org/10.1126/science.1058582
- Hoerling M.P., Hurrell J.W., Xu T., Bates G.T., Phillips. A (2004) Twentieth century North Atlantic climate change. Part II: understanding the effect of Indian Ocean warming. Clim Dyn 23, 391–405
- Huffman, G.J., A. Behrangi, D.T. Bolvin, E.J. Nelkin (2022), GPCP Version 3.2 Satellite-Gauge (SG) Combined Precipitation Data Set, Edited by Huffman, G.J., A. Behrangi, D.T. Bolvin, E.J. Nelkin, Greenbelt, Maryland, USA, Goddard Earth Sciences Data and Information Services Center [Accessed: 03/12/2024].]. https://doi.org/10.5067/MEASURES/GPCP/DATA304

- Hurrell J. W. (1995): Decadal trends in the North Atlantic Oscillation: Regional temperatures and precipitation. Science 269, 676-679. https://doi.org/10.1126/science.269.5224.676
- Hurrell J.W., Hoerling M.P., Phillips A.S., Xu T. (2004) Twentieth century North Atlantic climate change. Part I: assessing determinism. Clim Dyn 23:371–389
- Jeong, Y-C., Yeh S-W., Lim Y-K., Santoso A., and Wang G. (2022): Indian Ocean warming as key driver of long-term positive trend of Arctic Oscillation. NPJ Clim. Atmos. Sci. 5, 56, https://doi.org/10.1038/s41612-022-00279-x
- Johnson S.J., Stockdale, T. N., Ferranti, L., Balmaseda, M. A., Molteni, F., Magnusson, L., et al. (2019) SEAS5: The new ECMWF seasonal forecast system. Geosci. Model Dev. 12: 1087–1117. https://doi.org/10.5194/gmd-12-1087-2019
- Laloyaux, P., and Coauthors (2018). CERA-20C: A coupled reanalysis of the twentieth century. J. Adv. Mod. Earth Sys. 10, 1172–1195. https://doi.org/10.1029/2018MS001273
- Lee, R. W., Woolnough S. J., Charlton-Perez A. J., and Vitart F. (2019). ENSO modulation of MJO teleconnections to the North Atlantic and Europe. Geophysical Research Letters, 46, 13535–13545. https://doi.org/10.1029/2019GL084683
- Lee, S. H., Lawrence Z. D., Butler A. H., Karpechko A. Y. (2020). Seasonal forecasts of the exceptional northern hemisphere winter of 2020. Geophys. Res. Lett., 47(21). https://doi.org/10.1029/2020GL090328
- Lin H., Brunet G, and Derome J. (2009) An observed connection between the North Atlantic Oscillation and the Madden–Julian Oscillation. J Clim 22:364–380
- Molteni, F., and Brookshaw A. (2023): Early- and late-winter ENSO teleconnections to the Euro-Atlantic region in state-of-the-art seasonal forecasting systems. Clim. Dyn. 61, 2673–2692. https://doi.org/10.1007/s00382-023-06698-7
- Molteni, F., and Brookshaw A. (2024): Multi-decadal variability of tropical rainfall: reconciling ECMWF re-analyses and GPCP data. ECMWF Technical Memorandum no. 922 (available from: https://www.ecmwf.int/en/publications/technical-memoranda).
- Molteni F., Stockdale T. N., Vitart F. (2015) Understanding and modelling extra-tropical teleconnections with the Indo-Pacific region during the northern winter. Clim. Dyn. 45, 3119–3140. https://doi.org/10.1007/s00382-015-2528-y
- Molteni F., Roberts C.D., Senan R., Keeley S.P.E., Bellucci A., Corti S. et al. (2020) Boreal-winter teleconnections with tropical Indo-Pacific rainfall in HighResMIP historical simulations from the PRIMAVERA project. Clim. Dyn. 55, 1843–1873. https://doi.org/10.1007/s00382-020-05358-4
- Palmer, T.N. and Anderson D.L.T. (1994): The prospects for seasonal forecasting—A review paper. Q.J.R. Meteorol. Soc., 120, 755-793. https://doi.org/10.1002/qj.49712051802
- Raganato, A., Abid M.A., and Kucharski F. (2024): The combined link of the Indian Ocean dipole and ENSO with the North Atlantic-European circulation during early boreal winter in reanalysis and the ECMWF-SEAS5 hindcast. J. Climate. https://doi.org/10.1175/JCLI-D-23-0703.1
- Roberts, C., Senan R., Molteni F., Boussetta S., Mayer M., and Keeley S. (2018): Climate model configurations of the ECMWF Integrated Forecast System (ECMWF-IFS cycle 43r1) for HighResMIP. Geosci. Model Dev., 11, 3681–3712. https://doi.org/10.5194/gmd-11-3681-2018

- Roberts, C., Balmaseda M., Ferranti L. and Vitart F. (2023) Euro-Atlantic weather regimes and their modulation by troposphere and stratosphere teleconnection pathways in ECMWF re-forecasts. Mon. Wea. Rev., 151, 2779–2799. https://doi.org/10.1175/MWR-D-22-0346.1
- Saji, N., Goswami B., Vinayachandran P. et al. (1999) A dipole mode in the tropical Indian Ocean.

Nature 401, 360–363. https://doi.org/10.1038/43854

- Sanchez-Gomez E., Cassou C., Hodson D.L.R., Keenlyside N., Okumura Y., Zhou T. (2008) North Atlantic weather regimes response to Indian-western Pacific Ocean warming: a multi-model study. Geophys Res Lett 35, L15706. https://doi.org/10.1029/2008GL034345
- Stan, C., and Coauthors (2022): Advances in the Prediction of MJO Teleconnections in the S2S Forecast Systems. Bull. Amer. Meteor. Soc., 103, E1426–E1447. https://doi.org/10.1175/BAMS-D-21-0130.1
- Stockdale, T., Anderson D., Alves J. and Balmaseda M.A. (1998) Global seasonal rainfall forecasts using a coupled ocean–atmosphere model. Nature 392, 370–373. https://doi.org/10.1038/32861
- Trenberth, K.E. and Fasullo, J.T. (2013) An apparent hiatus in global warming? Earth's Future, 1, 19-32. https://doi.org/10.1002/2013EF000165
- Vautard, R., 1990: Multiple weather regimes over the North Atlantic: Analysis of precursors and successors. Mon. Wea. Rev., 118, 2056–2081. https://doi.org/10.1175/1520-0493(1990)118<2056:MWROTN>2.0.CO;2
- Vitart, F. , 2017: Madden–Julian oscillation prediction and teleconnections in the S2S database. Q. J. R. Meteorol. Soc. , 143, 2210–2220. https://doi.org/10.1002/qj.3079.
- Vitart, F. and Balmaseda M.A. (2024) Sources of MJO teleconnection errors in the ECMWF extended-range forecasts. Q. J. R. Meteorol. Soc., 150, 2028–2044. https://doi.org/10.1002/qj.4688
- Vitart, F. and Molteni F. (2010) Simulation of the Madden– Julian Oscillation and its teleconnections in the ECMWF forecast system. Q. J. R. Meteorol. Soc., 136: 842-855. https://doi.org/10.1002/qj.623
- Webster, P.J., Moore A.M., Loschnigg J.P., Leben R.R. (1999) Coupled ocean–atmosphere dynamics in the Indian Ocean during 1997–98. Nature 401, 356–360. https://doi.org/10.1038/43848
- Yadav, P. and Straus D.M. (2017): Circulation Response to Fast and Slow MJO Episodes, Mon. Wea. Rev., 145, 1577 – 1596. https://doi.org/10.1175/MWR-D-16-0352.1